Two stage tectonic history of the SW Amazon craton in the late Mesoproterozoic: identifying a cryptic suture zone

E. Tohver [a,*], B.A. van der Pluijm [a], K. Mezger [b], J.E. Scandolara [c,1], E.J. Essene [a]

[a] Department of Geological Sciences, University of Michigan, Ann Arbor, MI 48109-1063, USA
[b] Institut für Mineralogie, Universität Münster, Corrensstrasse 24, 48149, Münster, Germany
[c] Companhia de Pesquisas de Recursos Minerais (CPRM), Av. Lauro Sodré 2561, Porto Velho, RO 78904-300, Brazil

Abstract

The history of the SW Amazon craton during late Mesoproterozoic times is marked by two separate tectonic events, the first related to collision with southern Laurentia and the second caused by suturing of the Paragua craton. The polycyclic basement rocks of the SW Amazon craton exposed in the Brazilian state of Rondônia were deformed at lower amphibolite conditions during early Grenville times (ca. 1.2–1.15 Ga). This deformation episode is the last of several tectonometamorphic events that affected the granitoid rocks of the Amazon basement throughout the Mesoproterozoic. The southern margin of the Amazon craton during late Mesoproterozoic times is defined by the E–W trending Nova Brasilândia metasedimentary belt, where upper amphibolite to granulite facies rocks from a younger (ca. 1.09 Ga) collisional event are preserved. Temperature–time (T–t) paths for each domain (craton and metasedimentary belt) are constructed using U–Pb, $^{40}Ar/^{39}Ar$, and Rb–Sr data for minerals with different blocking temperatures. The T–t paths demonstrate no overlap in the timing or spatial distribution of tectonic and metamorphic activity. The separate cooling histories indicate the presence of a major tectonic boundary between the polycyclic basement rocks and the metasedimentary belt. This structure marks the suturing of the Paragua craton in the late Mesoproterozoic and is evidence that the accretionary history of the present outline of the Amazon craton was completed during the final stages of the amalgamation of Rodinia.
© 2005 Elsevier B.V. All rights reserved.

1. Introduction

Plate reconstructions for the Mesoproterozoic commonly propose a paleogeographic link between eastern Laurentia and the western margin of the Amazon craton (e.g., Hoffman, 1991; Weil et al., 1998). While the Amazon craton is traditionally defined by the Brasiliano belts that form its southeastern and eastern margins

* Corresponding author. Present address: Instituto de Geociências, Universidade de Sao Paulo Rua do Lago, 562, Sao Paulo, SP 05508-080, Brazil.
  E-mail address: etohver@usp.br (E. Tohver).
[1] Present address: Instituto de Geociências, Universidade de Brasília, CEP 70910-900, DF, Brazil.

(Almeida and Hasui, 1984), the temporal restrictions of this definition ignore the older, pre-Gondwanan history. One important aspect of documenting the accretionary and deformational history of the Amazon craton relates to the critical role played in the formation of the Precambrian supercontinent Rodinia; namely the collision between Amazonia and Laurentia during the Grenville orogeny (Rivers, 1997). Although there is general acceptance of this framework, the lack of detail regarding the tectonic history of the Amazon craton for the time interval 1.2–1.0 Ga hampers the assessment of tectonic links between the Amazon craton and Laurentia. The ability to critically evaluate Rodinia paleogeography is facilitated by comparing metamorphic histories, since metamorphism that is related to the collisional history can serve as a common element in the Rodinia framework. In the case of the exhumed Grenville orogen of Laurentia and the Amazon craton and its worldwide equivalents, the metamorphic history can be established through the study of the timing of peak meta-

morphism and subsequent cooling (e.g., Mezger et al., 1993; Ketchum et al., 1998; Rougvie et al., 1999).

Geochronological surveys of the SW Amazon craton began with the collection of whole rock Rb–Sr (Priem et al., 1971, 1989; Leal et al., 1978) and K–Ar data (Amaral, 1974). These geochronological data were originally interpreted in terms of linear, NW–SE trending domains that young to the SW (Teixeira et al., 1989; Sadowski and Bettencourt, 1996; Cordani and Sato, 1999). In the Brazilian state of Rondônia (Fig. 1), the use of modern geochronological techniques has improved the reliability of age data and the improvements in state infrastructure allow increased access to many outcrops. Recent studies based on U/Pb zircon age data coupled with Nd model ages have been expanded upon the original framework, although the increasing recognition of overlap between domains has raised questions regarding the exact locations of domain boundaries (Bettencourt et al., 1999; Pinho et al., 2003). The polycyclic nature of the SW Amazon basement
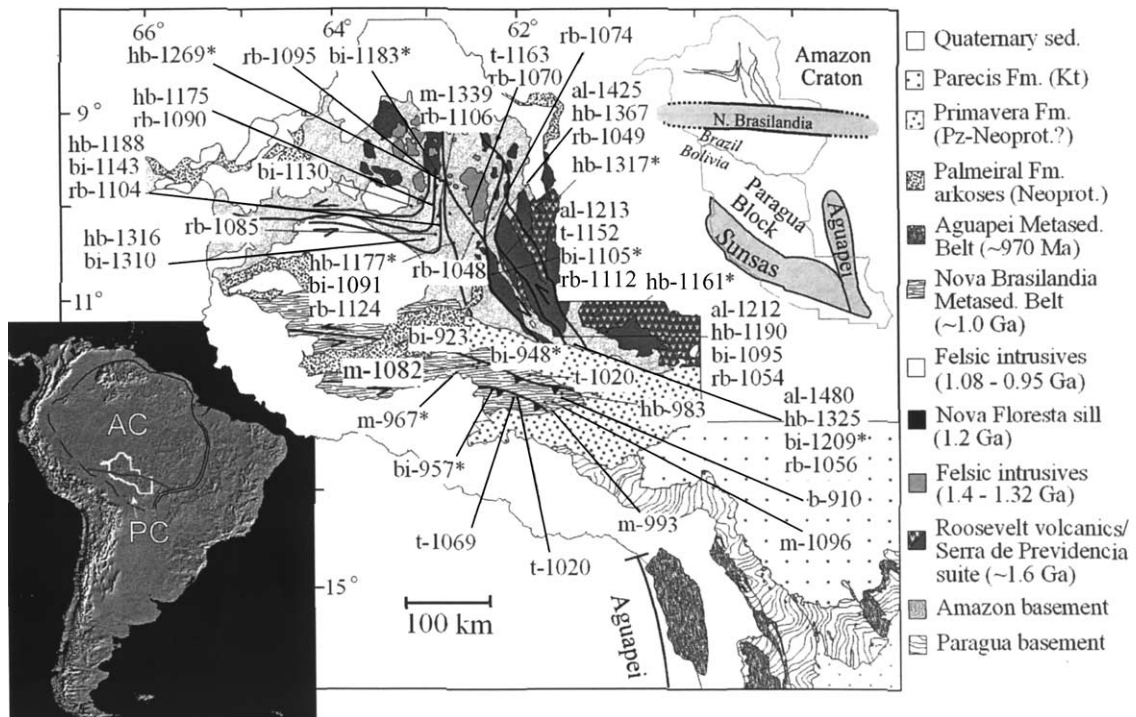

Fig. 1. Regional compilation of geochronological data from the Amazon craton and the adjacent Nova Brasilândia metasedimentary belt. Abbreviations are used as follows: m: monazite (U–Pb); al: allanite (U–Pb); t: titanite (U–Pb); hb: hornblende plateau (^{40}Ar/^{39}Ar); bi: biotite plateau (^{40}Ar/^{39}Ar); rb (Rb–Sr biotite). Asterisk denotes a total gas age.

is recognized from multiple episodes of intrusive activity throughout the Mesoproterozoic, while the abundance of U/Pb zircon ages and Nd model ages in the 1.8–1.5 Ga interval have been used to document crustal generation through processes interpreted to be anorogenic (Teixeira et al., 1989; Tassinari and Macambira, 1999). The focus of these studies on crust generating events, coupled with the refractory nature of igneous zircon, has given rise to an apparent contradiction of the Rodinia hypothesis; namely, the comparatively minor magmatic products of the 1.2–1.0 Ga interval do not reflect the widespread extent of Grenvillian deformation on the Amazon basement. Furthermore, the recent recognition of the Nova Brasilândia metasedimentary belt as a major Grenvillian mobile belt on the southern boundary of the SW Amazon craton basement (Rizzotto, 2001; Tohver et al., in press-a) requires a re-evaluation of previous Amazon craton tectonic models that correlate like-aged geological provinces across a fundamental tectonic boundary, the paleocratonic margin.

New U/Pb, $^{40}Ar/^{39}Ar$, and Rb/Sr data from the SW Amazon craton are used in this contribution to constrain the late Mesoproterozoic temperature-time (T–t) evolution of the SW Amazon craton, with particular emphasis on the amphibolite facies deformational event that occurred at 1.2–1.12 Ga. This T–t history is compared to that documented by Tohver et al. (2004) for the adjacent Nova Brasilândia metasedimentary belt in order to determine the duration and/or number of tectonometamorphic events that affected the SW Amazon craton during the late Mesoproterozoic. Comparable geochronological transects of the North American Grenville province reveal cases where a common, high grade metamorphic history is followed by separate, post-metamorphic cooling paths; indicative of the role of post-orogenic, extensional shear zones in the differential exhumation of orogenically-thickened crustal roots (e.g. Mezger et al., 1993; van der Pluijm et al., 1994; Ketchum et al., 1998). Other examples, also from the North American Grenville province, indicate wholly separate metamorphic histories, indicating separate geological terranes bounded by exhumed, reactivated suture zones (e.g. Mezger et al., 1992; Busch et al., 1997; Streepey et al., 2001). In this contribution, we document two temporally distinct and spatially separate orogenic events that occurred in the SW Amazon craton during late Mesoproterozoic times, reflec-

tive of 1) an early "Grenvillian" collision with southern Laurentia (Tohver et al., 2002; Tohver et al., in press) and 2) accretion of the Paragua craton to the Amazon craton (Tohver et al., 2004).

2. Geological setting

The basement geology of the SW Amazon craton, best exposed in the western Brazilian state of Rondônia, is commonly interpreted in terms of NW–SE trending crustal domains that young to the SW (Teixeira et al., 1989; Tassinari and Macambira, 1999; Tassinari et al., 2000). An alternative model for the Amazon craton, one that posits a dominantly Archean platform marked by anorogenic reactivation episodes, is discredited by the general lack of Archean ages (for review cf. Almeida and Hasui, 1984), although the emphasis on anorogenic processes has been adopted by many workers. The regional tectonic framework begins with the construction of the Rio Negro–Juruena magmatic arc (RNJ) at 1.85–1.6 Ga (Tassinari et al., 1996). Payolla et al. (2002) documented calc-alkaline affinities for tonalitic gneisses and enderbitic granulites that represent this arc in the central portion of the state of Rondônia, with ε_{Nd} initial values of −1.5 to +0.1, suggesting a continental arc setting with mantle-derived magmas. The emplacement of the voluminous subalkaline granites of the Serra da Providência suite at 1.60–1.53 Ma marks the end of this period of arc construction, which was accompanied by the intrusion of related charnockites, mangerites, and gabbros (Ouro Preto charnockite and Uniao Massif: U–Pb zircon ages, Bettencourt et al., 1999; SHRIMP ages from zircon, Tassinari et al., 1996). Rapakivi textures in many of these rocks are interpreted as indicating extensional tectonics related to cratonization at the end of the RNJ arc-building period. Supracrustal equivalents of the crystalline basement rocks are confined to the eastern portion of Rondônia, where the Roosevelt volcanosedimentary sequence records deposition in a shallow marine/continental regime. Volcanic rocks (pyroclastic flows and welded tuffs) from this sequence are dacitic to rhyolitic in composition and are interbedded with sedimentary rocks that include micaceous schists and iron formations (Leal et al., 1978; Rizzotto et al., 1995). A whole rock Rb–Sr isochron from this sequence yielded an age of 1560 ± 80 Ma

($^{87}Sr/^{86}Sr_0 = 0.701 \pm 0.005$), although the low-grade metamorphism that affected this sequence requires a cautious interpretation of this age (Tassinari, 1981). This supracrustal sequence is prominent in regional Radarsat images and appears to define an eastern limit to subsequent deformational episodes (Scandolâra et al., 1998).

The Rondoniano–San Ignacio orogenic province (1.5–1.3 Ga) was originally based on the age correspondence (Rb–Sr whole rock) between the basement rocks of the Paragua craton (Litherland et al., 1986, 1989) and basement rocks of central Rondônia (Teixeira et al., 1989). More recent U–Pb zircon work by Bettencourt et al. (1999) has identified the ages of emplacement of widespread felsic plutons into the basement of central Rondônia, most notably the ca.1.4 Ga Santo Antônio and Teotônio suites, the ca. 1.34 Ga Alto Candeias batholith, and the ca. 1.31 Ga São Lourenço–Caripunas suite. The U–Pb geochronology on basement rocks from western Mato Grosso by Geraldes et al. (1997, 2001) yielded ages of 1.48–1.42 Ga for the Santa Helena batholith, leading Tassinari et al. (2000) to suggest that the Paragua basement rocks from Bolivia/Mato Grosso are correlated with Amazon basement rocks in Rondônia. This suggested correlation will be examined in more detail later in this contribution.

The youngest of the episodes recognized in the SW Amazon craton basement is the 1.05–0.95 Ga Sunsas–Aguapeí event, which is equivalent in age to a major episode of Grenvillian deformation in North America. Magmatism associated with this event in the basement rocks of Rondônia is evidenced by the intrusion of the Santa Clara intrusive suite at ca. 1.08 Ga and a final pulse of tin-bearing granites, i.e., the Younger Granites of Rondônia, emplaced at high structural levels at 1.0–0.97 Ga. Deformation resulting from the orogenic event was originally considered to have been restricted to the bifurcated branches of the Sunsas/Aguapeí belt. The western limb, known as the Sunsas belt, is found in central Bolivia where Precambrian shield rocks are exposed. The Santa Catalina network of sinistral sense, strike–slip shear zones strikes NW over 500 km, and a subordinate system, the San Diablo network, displays a conjugate shear zone geometry with shear zone strikes ranging from NW to NE (Litherland and Bloomfield, 1981; Litherland et al., 1989). Abundant granitic intrusions (Casa de Piedras) were emplaced syn- to post-kinematically in the Sun-

sas belt at ca. 1.05 Ga, dated by Rb–Sr whole rock isochrons and K–Ar analyses of mica (Litherland et al., 1989). The eastern limb, known as the Aguapeí belt, is exposed in the western Brazilian state of Mato Grosso. Deformation of this belt is of minor extent (<50 km wide) and is observed chiefly as low-grade thrust faults verging to the SW (Barros et al., 1982). Fernandes (1999) identified strike–slip shear zones with dextral offsets that accompanied this deformation. Magmatic rocks are rare in the latter belt, with localized occurrences of a two-mica granite (São Domingos and Guapé intrusive suites) with zircon $^{207}Pb/^{206}Pb$ ages of ca. 930 Ma (Geraldes et al., 1997, 2001). The Sunsas belt is considered to mark the S boundary of the Paragua craton (Litherland et al., 1986; Teixeira et al., 1989). The aulacogenic origin of the Aguapei belt described by Saes (1999) indicates that the rocks on either side of the Aguapei belt have a common paleogeographic heritage as part of the Paragua craton. Recently, the recognition of the E–W trending Nova Brasilândia belt as a (1.1–1.0 Ga) collision zone affecting the late Mesoproterozoic margin of the SW Amazon craton places a northern limit on the extent of the Paragua craton (Rizzotto, 1999, 2001; Tohver et al., in press-a). The present study addresses the question of whether the ca. 1.1–1.0 Ga Nova Brasilândia deformation and metamorphism extended into the basement rocks of the SW Amazon craton.

3. Regional metamorphic history

The E–W trending Nova Brasilândia metasedimentary belt (NBMB) lies S of the exposed Amazon basement, with the actual contact covered by two sequences of Neoproterozoic to Paleozoic sediments (Leal et al., 1978; Scandolâra et al., 1998; Bahia, 1999). Given the abundant metapelitic assemblages that characterize the NBMB, *P–T–t* conditions of the area are well constrained (Tohver et al., in press-a). Widespread deformation and crustal thickening in this belt ($T_{max} = 750\,°C$, $P_{max} = 7.9$ kbars) was accompanied by the synkinematic emplacement of the Rio Branco granite at 1110 ± 15 Ma (U/Pb zircon, Rizzotto et al., 1999). Later emplacement of the Rio Pardo granite at 995 ± 15 Ma took place in the waning phases of deformation, as evidenced by weaker fabric development in these rocks (Rizzotto, 1999).

In contrast, the deformational and metamorphic history of the basement rocks of the SW Amazon craton immediately to the north of the NBMB is not as well resolved, especially compared with the general framework established above for igneous events. Unfortunately, the predominance of metaluminous granitoids in the basement rocks hampers detailed *P–T* studies, given the abundance of minerals such as biotite and hornblende and the absence of garnet. Therefore, it is difficult to distinguish between the exhumation history of the Amazon basement and the adjacent Nova Brasilândia metasedimentary belt by comparing pressure-constrained assemblages alone. Outside of prominent shear zones, basement rocks typically register lower amphibolite to granulite conditions, but there is no clear pattern in geographic distribution or temporal sequence. However, by determining the thermal history from geochronological systems with different blocking temperatures, a metamorphic and exhumation history for rocks on either side of the inferred boundary zone can be deduced. A polymetamorphic history has been suggested on the basis of variable resetting of the K–Ar system, which indicates a 1.3–0.95 Ga age range (Teixeira et al., 1989), with the youngest ages reflecting the limited thermal effects of the intrusion of the Younger Granites suite. More recent U–Pb (^{207}Pb/^{206}Pb monazite = 1326 ± 1 Ma) and Sm–Nd work (garnet-whole rock isochron 1309 ± 39 Ma) confirms the presence of the ca. 1.3 Ga metamorphic event (Payolla et al., 2002), possibly related to the thermal effects of granite emplacement (Tassinari et al., 2000). Widespread 1.18–1.12 Ga deformation at 450–550 °C has been demonstrated in association with large shear zones, as evidenced by ^{40}Ar/^{39}Ar dating and feldspar thermometry (Bettencourt et al., 1996; Tohver et al., in press-b) from the well-exposed central portion of the state of Rondônia.

4. Geochronology

A combination of U/Pb, ^{40}Ar/^{39}Ar, and Rb–Sr analyses was conducted on 29 samples to constrain the high (700–600 °C), medium (500–300 °C) and low temperature (ca. 300 °C) cooling history of the basement rocks of the SW Amazon craton. Geochronological results and sample locations are presented in Table A.1 in

Appendix A. Separates of U-bearing minerals such as monazite, allanite and titanite were dated with conventional U–Pb, isotope dilution techniques at Universität Münster (for description of U/Pb methods see Tohver et al., in press-a), complemented with ^{40}Ar/^{39}Ar analysis of hornblende and biotite at the University of Michigan (for description of ^{40}Ar/^{39}Ar methods see Tohver et al., 2002). Analysis of 10–15 mg separates of biotite for Rb–Sr was performed at the Universität Münster in order to constrain the younger cooling history (~300 °C), as well as for comparison with ^{40}Ar/^{39}Ar biotite ages. Biotite samples were lightly ground in an agate mortar and sieved to remove non-phyllosilicate impurities. Sample were dissolved overnight in a HF–HNO$_3$ mixture with a ^{87}Rb–^{84}Sr spike in sealed, screw-op Savillex vials in Teflon-lined bombs. Rb and Sr were separated by standard ion exchange procedures in quartz columns using 2.5N HCl as eluent. Tantalum filaments were used for loading Rb, which was measured on a Teledyne mass spectrometer. Tungsten filaments were used for Sr mass spectrometric analysis, measured on a VG Sector 54 multi-collector mass spectrometer. Correction for mass fractionation is based on a ^{86}Sr/^{88}Sr ratio of 0.1194. Rb ratios were corrected for mass fractionation using a factor deduced from multiple measurements of Rb standard NBS 607.

The U/Pb analyses of monazite and allanite (Fig. 2), with blocking temperatures of ca. 700 and 650 °C,
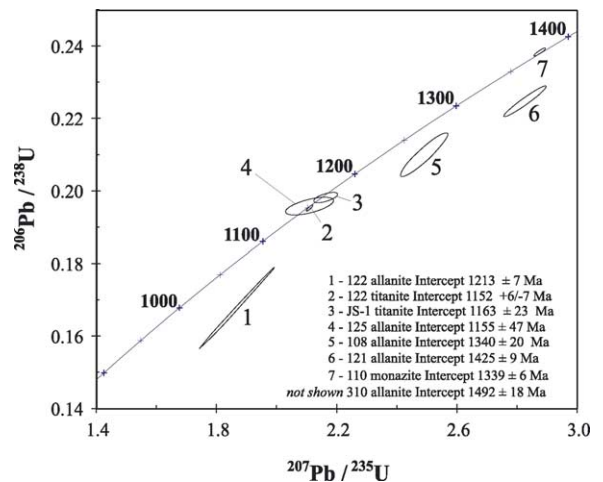

Fig. 2. U–Pb concordia plots for minerals analyzed from the Amazon basement of central Rondônia. The U/Pb ages (listed) for discordant samples are determined by a line through the origin and the intercept with the U/Pb concordia curve.

respectively (Parrish, 1991; Heaman and Parrish, 1991), demonstrate a relict, high-grade history with ages of ca. 1.35 Ga, similar to $^{40}Ar/^{39}Ar$ ages preserved in hornblende from undeformed samples (Table 1). Allanite grains are typically discordant, with the 1.35 Ga age inferred from $^{207}Pb/^{206}Pb$ ratios after correction for common Pb. Younger, discordant allanite grains with ca. 1.2 Ga ages are found in sheared rocks, indicating isotopic resetting through deformation, as interpreted for reset hornblende ages. Titanite grains typically record this ca. 1.2 Ga deformation with ages 1155 ± 6 and 1195 ± 23 Ma, also from rocks that have been recrystallized during deformation (Fig. 2).

Hornblende ages from $^{40}Ar/^{39}Ar$ analysis reveal two principal age ranges (see representative argon isotope data in Table A.2 in Appendix A). Ages of ca.1.35 Ga are found in rocks not directly deformed by the Ji-Paraná shear zone network, whereas a younger set of ages in the 1.18–1.12 Ga range are observed in mylonitic to protomylonitic samples. All biotite samples from both shear zones and undeformed rocks yield ages in the younger 1.15–1.10 Ga range, indicating that the temperature of regional deformation during this younger deformation event (1.2–1.12 Ga) was sufficiently hot to thermally reset biotite, which therefore, represent cooling ages. The exception to this pattern is sample Ron103, in which biotite grains yield ages older than the coexisting hornblende, suggesting the incorporation of excess ^{40}Ar (Fig. 3). The hornblende grains from this sample are characterized by a saddle-shaped spectrum, a feature also indicative of excess argon (Table A.1). Age data from this sample are considered as meaningless and are not considered in the discussion to follow.

The Rb–Sr analysis of biotite was undertaken to test the significance of $^{40}Ar/^{39}Ar$ ages and address the possibility of widespread, unrecognized excess ^{40}Ar. Both radiogenic daughters (^{40}Ar and ^{87}Sr) have a closure temperature of $\sim300\,°C$, making these systems ideal complements in establishing the chronology of cooling below the inferred temperature of deformation. A very wide distribution in $^{87}Rb/^{86}Sr$ compositions for biotite samples is seen in Fig. 4 with tight clustering about a regressed line (slope $= 0.01576 \pm 0.00012$, initial $^{87}Sr/^{86}Sr = 0.70432 \pm 0.00018$, MSWD $= 0.9865$) from which an age of 1101 ± 9 Ma can be calculated. The initial $^{87}Sr/^{86}Sr$ from the regression is in good agreement with the 0.704–0.723 range previously

Table 1
U–Pb analyses

Sample	U (ppm)	Pb (ppm)	$^{208}Pb/^{206}Pb$	$^{206}Pb/^{204}Pb$	$^{207}Pb/^{206}Pb$	Error	$^{207}Pb/^{235}U$	Error	$^{206}Pb/^{238}U$	Error	Rho	Age data (Ma)		
												$^{206}Pb/^{238}U$	$^{207}Pb/^{235}U$	$^{207}Pb/^{206}Pb$
122 t	279.1	57.5	0.066	789.508	0.07833	0.0002	2.108	0.009	0.195	0.001	0.870	1148	1149	1152
122 al	603.6	432.6	3.784	906.934	0.08074	0.0002	1.866	0.103	0.168	0.009	0.999	998.0	1068	1213
108 al	250.4	640.5	12.252	108.144	0.08598	0.0008	2.489	0.064	0.210	0.005	0.926	1222	1258	1320
125 al	169.2	693.9	19.604	52.969	0.0806	0.002	2.339	0.065	0.210	0.002	0.630	1204	1185	1150
js1 t	227.6	89.17	0.241	86.649	0.0799	0.001	2.212	0.033	0.201	0.001	0.633	1165	1165	1163
110 mon	2119	1584	2.602	3910.641	0.08604	0.0001	2.766	0.010	0.233	0.001	0.914	1351	1346	1339
121 al	75.41	445.7	29.505	376.460	0.09014	0.0003	2.752	0.039	0.221	0.003	0.964	1288	1340	1425
310 al	271.1	397.9	3.953	88.172	0.09373	0.0009	3.671	0.061	0.284	0.003	0.800	1610	1560	1492

Abbreviations: mon, monazite; t, titanite; al, allanite. Multigrain aliquots were handpicked from heavy liquid separates using a binocular microscope. Monazite analyses comprised 3–5, $\sim$50–300 μm grains and titanite analyses 0.5–3 mg aliquots of $\sim$30–500 μm grains. All errors are calculated at the 2σ level. Mass fractionation was determined to be 1.001 per atomic mass unit and analytical blanks ranged from 30 to 120 pg Pb. Initial Pb was calculated according using Stacey and Kramers (1975) two-stage Pb evolution model with a μ_2 value of 10.0, according to the findings of Tohver et al. (2004).
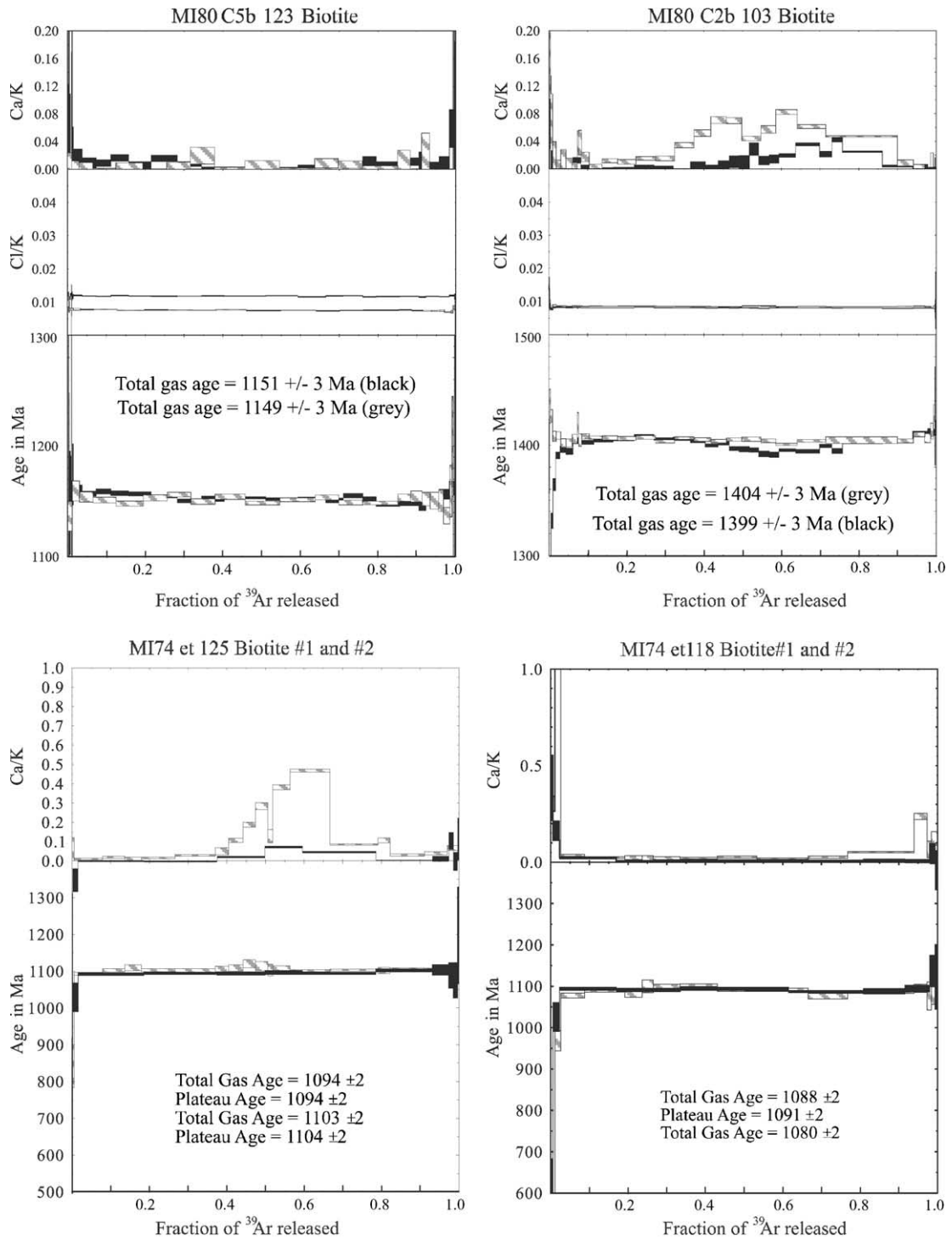
Fig. 3. Argon age spectra from the Amazon basement samples. Ca/K and Cl/K ratios are also indicated for samples, in order to demonstrate possible effects of composition on the calculated age, notably observed in hornblende sample Ron314.
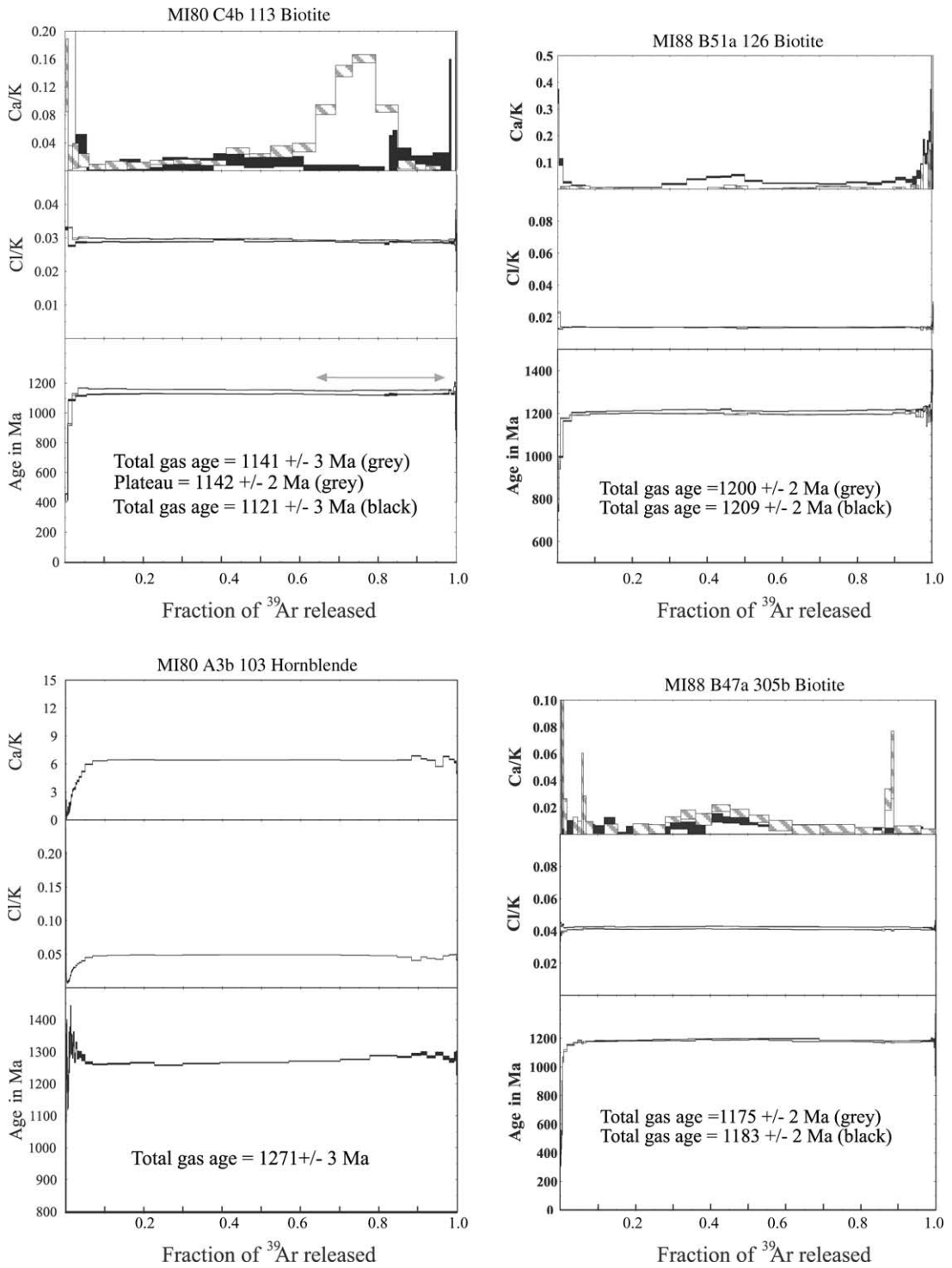
Fig. 3. (*Continued*)
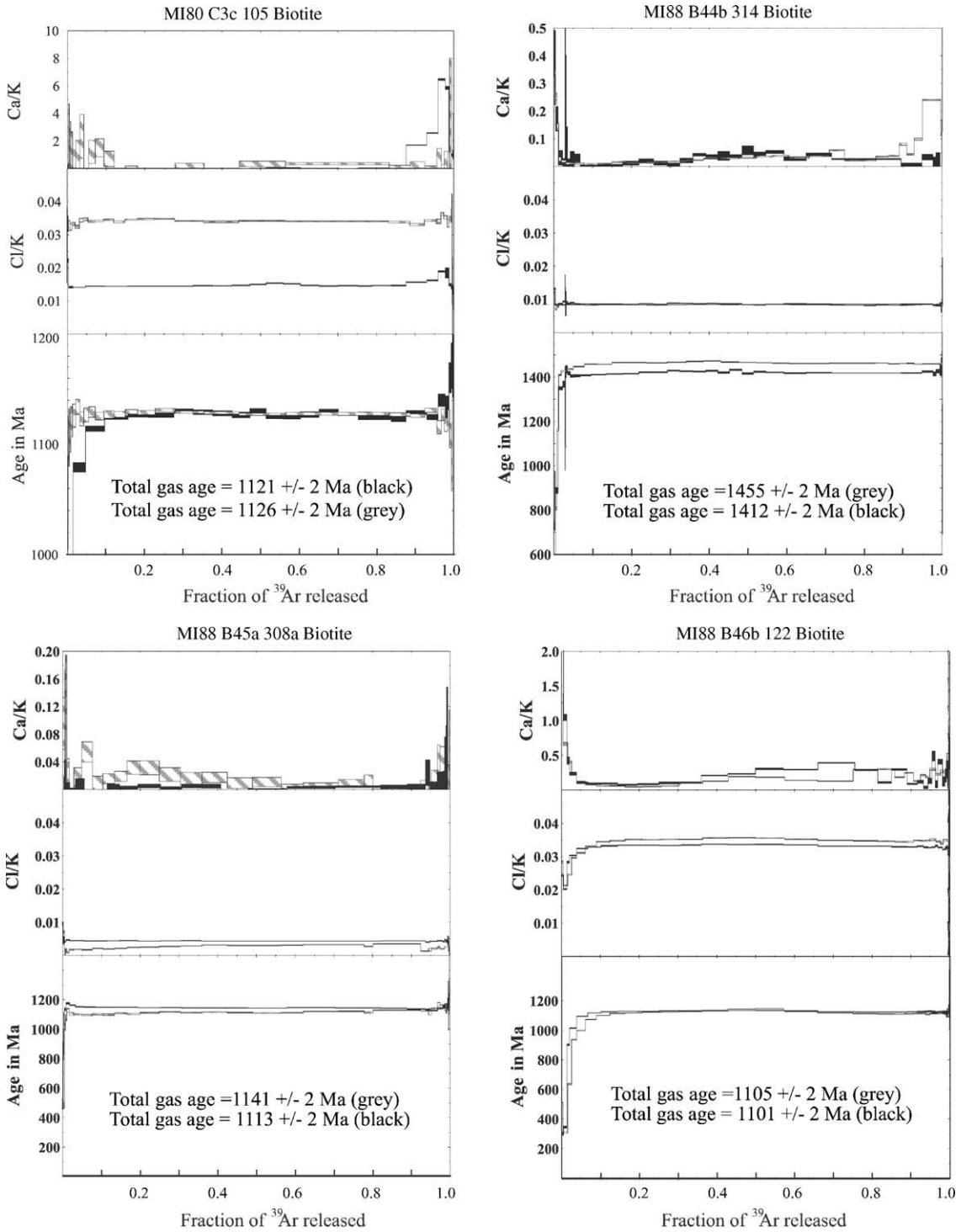
Fig. 3. (*Continued*)
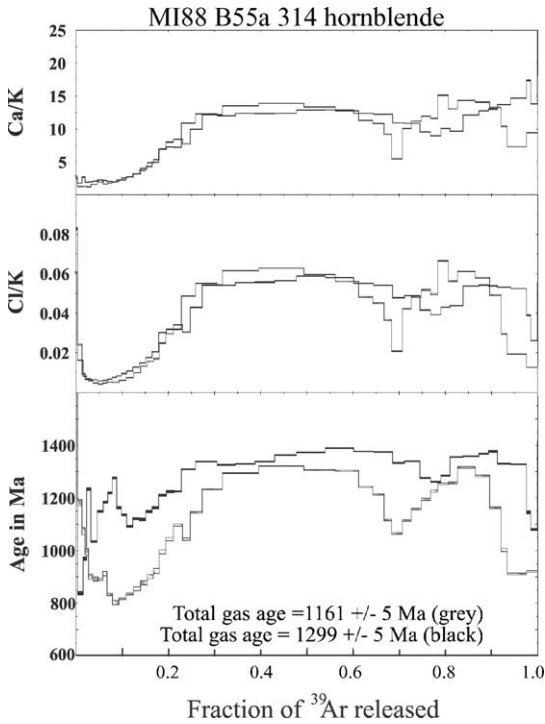
Fig. 3. (*Continued*).

reported by Priem et al. (1989) and Tosdal and Bettencourt (1994). It is unlikely that a single, initial $^{87}Sr/^{86}Sr$ value is strictly valid for all rock samples, taken from tens to hundreds of kilometers apart, as would be implied by using the initial value determined by a regressed line through all samples. On this regional sampling scale, isotopic heterogeneities with regard to the initial value signify that the age calculated from this 'errorchron' represents the average metamorphic cooling age of all samples. With this caveat in mind, we use the $^{87}Sr/^{86}Sr$ determined from this regression to calculate model ages for individual samples (see Table 2). In general, there are two sources of uncertainty for model ages thus calculated: first, instrumental precision in the determination of $^{87}Rb/^{86}Sr$ and $^{87}Sr/^{86}Sr$ (principally the former, compare $\pm\ ^{87}Rb/^{86}Sr$ versus $\pm\ ^{87}Sr/^{86}Sr$ in Table 2); and second, error related to incorrect Sr_0 values for individual samples (Davidson et al., 2005). The latter source of error decreases proportionally to the $^{87}Sr/^{86}Sr$; compare $^{87}Sr/^{86}Sr$ values with ΔAge column in Table 2. To test the geological significance of the model ages, we assume that the age of the reference isochron is a time of uniform regional cooling. If this assumption were true, all variation in
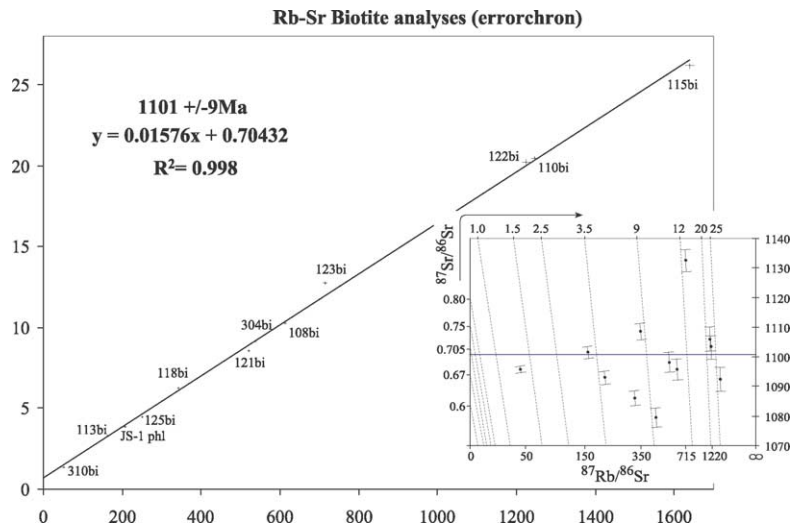
Fig. 4. Rb–Sr analyses for mica grains from the Amazon basement rocks of central Rondônia. Conventional isochron diagram yields a well-fit line from sample data points depicted with associated error bars. A better representation of the true error associated with each data point is shown with the isochron diagram devised by Provost (1990), where samples are depicted in the same relative order, left to right, on a graduated scale for the abscissa $^{87}Rb/^{86}Sr$. Values depicted on the ordinate (projected to the upper axis) are graduated in terms of initial $^{87}Sr/^{86}Sr$, and are calculated as a parameterized function of both $^{87}Rb/^{86}Sr$ and $^{87}Sr/^{86}Sr$, with oblique lines depicting constant values for total $^{87}Sr/^{86}Sr$. The horizontal line is the regressed line shown in the conventional isochron diagram, with samples yielding older and younger model ages plotting above the line and below the line, respectively, in a fashion similar to the conventional isochron diagram.

Table 2
Rb–Sr analyses

Sample	Rb (ppm)	Sr (ppm)	$^{87}Rb/^{86}Sr$	±	$^{87}Sr/^{86}Sr$	±	Age (Ma) $Sr_0 = 0.704$	ΔAge (Ma) $Sr_0 = 0.75$	2σ
Ron 118 biotite	602.63	7.81	344	0.9	6.241	0.0001	1124	−10	3
Ron 304 biotite	837.60	8.22	537	3	9.120	0.0017	1095	−7	6
Ron 123 biotite	707.76	6.23	715	1	12.732	0.0003	1175	−5	2
Ron 122 biotite	855.96	5.88	1225	4	20.210	0.0006	1112	−3	4
Ron 110 biotite	690.37	4.70	1247	5	20.456	0.0016	1106	−3	4
JS-1 phlogopite	789.10	14.44	207	2	3.889	0.0001	1070	−17	5
Ron 125 biotite	707.09	11.22	249	2	4.463	0.0001	1054	−14	4
Ron 310 biotite	505.64	31.77	49.4	0.4	1.451	0.0000	1056	−70	20
Ron 113 biotite	760.36	16.94	163	1	3.277	0.0001	1106	−21	6
Ron 121 biotite	833.61	8.15	523	4	8.550	0.0002	1049	−7	2
Ron 108 biotite	835.44	7.63	613	5	10.269	0.0000	1090	−6	2
Ron 115 biotite	1196.74	7.37	1639	10	26.158	0.0001	1085	−2	1

Rb–Sr and age data for biotite separates from the SW Amazon craton basement rocks. Errors reported for $^{87}Rb/^{86}Sr$ and $^{87}Sr/^{86}Sr$ are at the 2σ level. Ages in Ma are calculated assuming $Sr_0 = 0.704$. The column entitled "Δage (Ma) $Sr_0 = 0.75$" shows the change in the calculated age, assuming $Sr_0 = 0.75$. The column "2σ" shows the error in the age calculation, based on precision in the measured isotopic values of Sr and Rb.

calculated model ages would be due to heterogeneities in the initial $^{87}Sr/^{86}Sr$ value for individual samples. This exercise reveals that an improbably high variation in initial $^{87}Sr/^{86}Sr$ values would be required to explain the differences between individual model ages (e.g., $^{87}Sr/^{86}Sr_0 > 1.45$ for sample Ron 123), as seen from the Provost-type isochron plot (inset, Fig. 4),. This observation indicates that the variation in Rb–Sr model ages reflects geological events, rather than just localized heterogeneities of initial $^{87}Sr/^{86}Sr$ from sample to sample.

The combination of U–Pb, $^{40}Ar/^{39}Ar$, and Rb–Sr geochronological techniques demonstrates the effects of at least two metamorphic events that affected the basement rocks of the SW Amazon craton. The tectonic significance of the older, 1.35 Ga metamorphism is uncertain, although the abundant magmatic products that mark this period may indicate a heat source for static crustal metamorphism (Payolla et al., 2002) and extensive U mobilization (Tohver et al., 2004). In contrast, the resetting of isotopic systems during the 1.2–1.12 Ga interval is clearly associated with the effects of deformation (e.g., strain induced recrystallization in shear zones) that cannot have been operative at temperatures greater than ca. 500 °C, otherwise all hornblende samples would record cooling ages <1.2 Ga. The clustering of biotite ages at ≤1150 Ma for both the Rb–Sr and $^{40}Ar/^{39}Ar$ systems indicates

that the temperature of regional deformation was sufficient to thermally reset all biotite samples, i.e., these are cooling ages that follow the younger ca. 1.2–1.15 Ga deformation.

5. Discussion

Geochronological constraints on the metamorphic history of the SW Amazon craton demonstrate the widespread effects of deformation during the late Mesoproterozoic. The 1.2–1.1 Ga deformation (early Grenville) affects a basement complex of metaigneous granitoids and metavolcanics with a history that is commonly 300–600 My older. The basement rocks were affected by at least one widespread metamorphic event before the early Grenville deformation, possibly the result of widespread felsic intrusions at ca. 1.43–1.35 Ga (Payolla et al., 2002). Metamorphic minerals dated by the $^{40}Ar/^{39}Ar$ and U–Pb techniques reveal a bimodal distribution of ages, the ca. 1.35 Ga event and a younger set of ca.1.2–1.15 Ga ages. Hornblendes dated by $^{40}Ar/^{39}Ar$ analysis replicate this pattern, with the younger age range representing the timing of deformation of sheared rocks. The preservation of the older hornblende ages in less deformed blocks points to the role of deformational processes, rather than cooling below the argon closure temperature, as being chiefly re-

sponsible for isotopic age resetting. Thus, the variation in deformation ages is ascribed to episodic reactivation of mylonitic shear zones (Tohver et al., in press-b). Biotites dated by either $^{40}Ar/^{39}Ar$ or Rb–Sr analysis always record ages that correspond to the younger 1.2–1.15 Ga deformation event or cooling in the wake of that episode.

The geological history of the Amazon basement is of a long-lived, polycyclic nature, whereas the adjacent Nova Brasilândia metasedimentary belt appears to have experienced a single Wilson cycle, i.e., production of mafic crust associated with deep water sediments, followed by crustal thickening through collision and the syn- to post-collisional intrusion of granites (Tohver et al., in press-a). The sedimentary protolith of the collision zone mostly comprises metamorphosed greywackes and marls interpreted as turbidite flows on a marine shelf-slope environment (Rizzotto, 1999), clearly distinct from the crystalline metaigneous rocks of the polycyclic basement rocks to the N. Comparison of the metamorphic history of the two domains juxtaposed at the surface today reveals two separate records that are temporally and spatially distinct. Cool-

ing of the SW Amazon craton basement rocks and the adjacent Nova Brasilândia metasedimentary belt took place along two separate T–t trajectories that do not overlap (Fig. 5). The lack of a common history at the highest grades (Amazon $T_{deformation} \leq 500\,^{\circ}C$, Nova Brasilândia $T_{metamorphism} \sim 700$–$750\,^{\circ}C$) demonstrates that the timing of peak tectonometamorphism took place 60–100 Ma apart. Furthermore, the lack of a common cooling trend even at the closure temperature of biotite (ca. 1050 Ma for craton versus 950 Ma for Nova Brasilândia Metasedimentary Belt) signifies that the juxtaposition of the different crustal levels exposed in the Amazon basement rocks and the adjacent Nova Brasilândia belt is the result of differential uplift later in the Neoproterozoic. The deposition of arkosic sediments of the Palmeiral Formation onto both of these domains provides a common, albeit radiogenically undated surface exposure age for both. The Nova Brasilândia mobile belt serves as the boundary between the SW Amazon craton basement and the adjacent Paragua craton, two cratonic blocks with no geological connection required before the suturing at ca. 1.1 Ga. This suture zone interpretation draws on
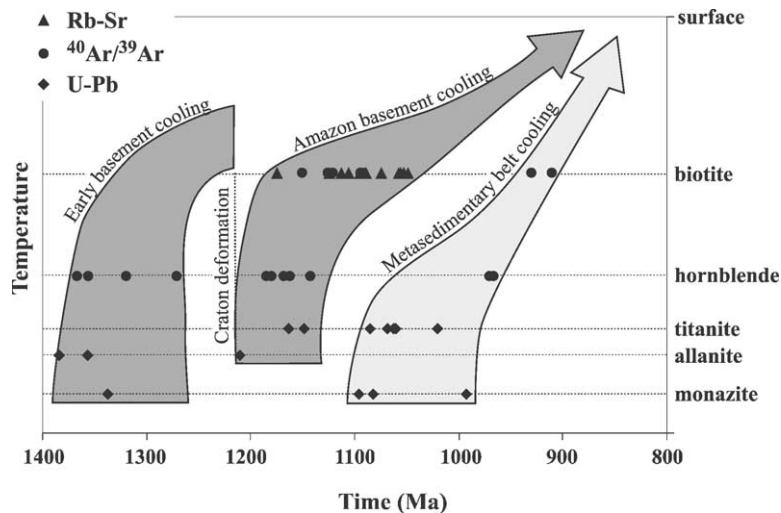
Fig. 5. Composite temperature–time path for SW Amazon craton. The polycyclic basement exhibits a polymetamorphic history with final cooling following deformation during 1.2–1.15 Ga event (dark grey) resulting from collision with southern Laurentia. The Nova Brasilândia metasedimentary belt (light grey) has a separate evolution with no evidence for metamorphic history prior to 1.1 Ga, meaning that the protolith for the Nova Brasilândia belt was not in place until after deformation of the adjacent basement rock had ceased. Thus, the two-stage tectonometamorphic history of the SW Amazon craton includes early "Grenvillian", strike–slip basement deformation at ca. 1.2–1.15 Ga, followed by deposition and subsequent deformation/metamorphism at 1.1 Ga when the final docking of the Paragua craton took place.

observations of the dismembered layered mafic rocks and marine sediments that form the NBMB protolith, relicts of an ocean basin that were reworked during the collision with the Paragua craton (Tohver et al., in press-a).

The two-stage history, and the identification of a ca. 1.10 Ga Nova Brasilândia suturing belt in the SW Amazon craton has clear significance for Rodinia paleogeography, particularly for the number and identity of the cratons colliding with the Grenville margin of Laurentia. Many workers have recognized the ca. 1.15 Ga Elzeviran and 1.05 Ga Ottawan orogenies as tectonic pulses in the central portion of the Grenville Province (Davidson, 1998). However, the suggestion that the Amazon craton was responsible for both episodes is not supported by paleomagnetic evidence suggesting that the Amazon craton collided with the southernmost portion of the Grenville Province of Laurentia (Llano region, Texas) at ca. 1.2 Ga (Tohver et al., 2002). New models for Grenville tectonics, therefore, need to account for the early ca. 1.2 Ga Amazon–Llano fit and continued relative motion between the two cratons after the initial collision. It has been proposed that a component of sinistral strike–slip motion of the Amazon craton resulted in a more northerly (modern coordinates) position against the central Grenville Province of Ontario and New York (Tohver et al., in press-a). This could explain the second, 1.05 Ga Ottawan orogeny as caused by emplacement of Amazonia. Additional evidence for the strike–slip passage is provided by Carrigan et al. (2003), who demonstrated non-Laurentian zircon ages in suspect Grenville inliers in the southern Appalachians. Loewy et al. (2003) and Tohver et al. (2004) extend these observations to propose an Amazonian provenance for these SE Appalachian rocks, although different paleogeographic scenarios preceding the transfer of Amazonian crust are inferred by these authors. The origin of the 1.15 Ga tectonic pulse in the central Grenville Province of Laurentia requires collision with another tectonic block, either a terrane or continent, possibly Baltica or the Paragua craton itself.

6. Conclusions

A two-stage tectonic history for the SW Amazon craton during the Grenville interval (1.2–1.0 Ga) is inferred from geochronological results obtained in this study. The Paleoproterozoic cratonic rocks preserve ca. 1.35 Ga metamorphic ages (U–Pb monazite and allanite, ^{40}Ar/^{39}Ar hornblende) that were overprinted in some places by deformation. Deformation took place at ca. 1.2–1.15 Ga (U–Pb allanite and titanite, ^{40}Ar/^{39}Ar hornblende) with cooling from this event recorded in all sample localities by ^{40}Ar/^{39}Ar and Rb–Sr analysis of biotite. The adjacent Nova Brasilândia metasedimentary belt preserves a younger metamorphic (<1.10 Ga) history related to crustal thickening. The separate tectonometamorphic histories and observations of mafic rocks (oceanic crust?) and marine sediments are interpreted to indicate the presence of a suture marking the collision between the SW Amazon craton and the Paragua craton at the end of Mesoproterozoic times. The existence of this suture belt indicates that the initial docking of the Amazon craton with southern Laurentia at 1.2 Ga was followed by strike–slip motion, allowing for later suturing of the Paragua craton in the final stages of the amalgamation of Rodinia.

Appendix A

See Tables A.1 and A.2.

Table A.1
Geochronological results and sample locations

Sample	Location	U–Pb	$^{40}Ar/^{39}Ar$	Rb/Sr biotite (assuming $Sr_0 = 0.704$)
103	9°51.68′S63°7.86′W	–	1265 ± 3 hb*, 1271 ± 3 hb*, 1269 ± 3 hb, 1404 ± 3 bio*, 1399 ± 3 bio*, excess Ar(?)	–
105	9°59.17′S63°8.02′W	–	1126.2 ± 2.4 bio*, 1130 ± 3 bio	–
107	10°17.66′S63°19.19′W	–	1368 ± hb*, 1310 ± 3 bio*	–
108	9°58.51′S63°2.24′W	1338 ± 19 al	1168 ± 3 hb*, 1175 ± 3 hb	1090 ± 2
110	10°4.70′S62°58.39′W	1339 ± 6 m	–	1106 ± 4
113	10°9.143′S62°50.54′W	–	1185 ± 4 hb*, 1188 ± 5 hb, 1161 ± 4 hb*, 1141 ± 3 bio*, 1143 ± 3 bio, 1121 ± 3 bio*, 1126 ± 3 bio	1106 ± 6
115	10°10.47′S62°54.60′W	–		1085 ± 1
118	10°17.75′S62°46.26′W	–	1245 ± 2 hb*, 1177 ± 2 hb*, 1088 ± 2 bio*, 1091 ± 2 bio, 1080 ± 2 bio*	1124 ± 3
119	10°22.262′S62°33.48′W		1356 ± 3 hb*, 1317 ± 3 hb*	–
121	10°31.85′S62°23.86′W	1429 ± 9 al	1367 ± 3 hb*, 1367 ± 3 hb, 1328 ± 3 hb*	1049 ± 2
122	10°36.112′S62°20.69′W	1215 ± 7 al	1105 ± 2 bio*	1112 ± 4
123	10°42.52′S62°15.38′W	1155 ± 7 t	1142 ± 5 hb*, 1155 ± 5 hb, 1243 ± 3 hb*, 1149 ± 3 bio*	1175 ± 2
125	11°9.41′S61°54.01′W	1212 ± 45 al	1310 ± 5 hb*, 1190 ± 6 hb, 1094 ± 2 hb*, 1094 ± 2 bio, 1103 ± 2 bio*, 1104 ± 2 bio	1054 ± 6
126	11°10.93′S61°54.17′W	–	1318 ± 3 hb*, 1325 ± 4 hb, 1348 ± 3 hb*, 1335 ± 5 hb, 1209 ± 2 bio*	–
127	11°40.69′S62°11.88′W	–	930 ± 3 hb*, 928 ± 4 bio, 923 ± 3 bio*, 920 ± 3 bio	–
133	11°54.60′S61°46.82′W	–	994 ± 6 hb*, 983 ± 7 hb, 1005 ± 7 hb*	–
134	11°54.90′S61°46.79′W	1090 ± 6 m	912 ± 2 hb*, 910 ± 2 bio, 914 ± 2 bio*	–
135	11°55.79′S62°02.17′W	–	961 ± 4 hb*, 966 ± 3 hb	–
303	9°47.78′S62°55.60′W	–	1307 ± 2 hb*	–
304	9°47.84′S62°54.25′W	–	–	1095 ± 4
305	9°46.92′S62°53.69′W	–	1183 ± 2 bio*	–
308	10°24.85′S62°30.36′W	–	1067 ± 2 hb*, 1096 ± 2 hb*, 1113 ± 2 bio*	–
310	11°10.96′S61°54.09′W	–	–	1056 ± 4
314	11°24.05′S61°19.25′W	–	1161 ± 5 hb*, 1299 ± 5 hb*, 1455 ± 2 bio*	–
316	11°49.32′S61°51.05′W	1020 ± 15 m	–	–
319	11°57.46′S61°51.15′W	993 ± 12 m	–	–
324a	11°48.76′S62°18.78′W	–	964 ± 1 bio*	–
325	11°48.84′S62°18.63′W	–	957 ± 2 bio*	–
326	11°40.76′S62°11.78′W	1082 ± 6 m	948 ± 2 bio*	–

m, Monazite; al, allanite; t, titanite; hb, hornblende; bio, biotite; *, total gas age, otherwise plateau age.

Table A.2
Representative argon isotope data

Power	Fraction	$^{40}Ar/^{39}Ar$	$^{38}Ar/^{39}Ar$	$^{37}Ar/^{39}Ar$	$^{36}Ar/^{39}Ar$	$^{40}Ar*/^{39}Ar$	%atm	Ca/K	Age (Ma)	1σ error
d4b biotite et118										
50	0.006	15.352	0.053	0.209	0.000	15.470	−0.763	0.209	533	150
100	0.017	35.632	0.030	0.089	0.004	34.437	3.355	0.089	1026	35
200	0.147	37.372	0.026	0.011	0.000	37.490	−0.315	0.011	1094	4
275	0.166	37.389	0.024	0.003	0.000	37.356	0.089	0.003	1091	5
350	0.167	37.381	0.025	0.004	0.000	37.492	−0.297	0.004	1094	4
425	0.113	37.234	0.024	0.004	−0.001	37.428	−0.520	0.004	1093	5
500	0.193	37.124	0.024	0.003	0.000	37.179	−0.148	0.003	1087	3
600	0.107	37.032	0.024	0.004	−0.001	37.211	−0.484	0.004	1088	7
675	0.064	37.014	0.025	0.002	−0.002	37.499	−1.311	0.002	1094	8
800	0.013	37.450	0.024	0.024	−0.007	39.473	−5.402	0.024	1137	38
3000	0.007	37.149	0.034	−0.024	−0.006	38.779	−4.386	−0.024	1122	78

J-value = 0.02224 ± 0.00004
Total gas age 1088.2 ± 2.4 Ma

Table A.2 (*Continued*)

Power	Fraction	$^{40}Ar/^{39}Ar$	$^{38}Ar/^{39}Ar$	$^{37}Ar/^{39}Ar$	$^{36}Ar/^{39}Ar$	$^{40}Ar^*/^{39}Ar$	%atm	Ca/K	Age (Ma)	1σ error
C4a-113 bio										
100	0.005	8.154	1.662	0.074	0.007	6.124	24.895	0.074	422	23
200	0.011	15.780	0.157	0.005	0.002	15.331	2.847	0.005	914	7
250	0.015	20.050	0.140	0.011	0.001	19.901	0.744	0.011	1116	6
300	0.026	20.805	0.142	0.007	0.000	20.940	−0.651	0.007	1159	3
350	0.042	20.716	0.141	0.000	0.000	20.794	−0.377	0.000	1153	2
400	0.055	20.705	0.140	0.003	0.000	20.843	−0.665	0.003	1155	2
450	0.059	20.710	0.141	0.003	0.000	20.748	−0.185	0.003	1151	1
500	0.060	20.709	0.140	0.006	0.000	20.716	−0.035	0.006	1149	1
550	0.068	20.726	0.141	0.006	0.000	20.730	−0.022	0.006	1150	2
600	0.066	20.674	0.140	0.005	0.000	20.731	−0.277	0.005	1150	2
650	0.060	20.626	0.141	0.015	0.000	20.633	−0.035	0.015	1146	1
700	0.054	20.654	0.140	0.011	0.000	20.658	−0.019	0.011	1147	1
750	0.056	20.673	0.140	0.014	0.000	20.638	0.170	0.014	1146	2
800	0.059	20.580	0.138	0.017	0.000	20.565	0.073	0.017	1143	2
850	0.051	20.499	0.138	0.047	0.000	20.502	−0.011	0.047	1141	2
900	0.043	20.515	0.137	0.077	0.000	20.480	0.173	0.077	1140	2
950	0.060	20.584	0.139	0.087	0.000	20.586	−0.011	0.087	1144	2
1000	0.058	20.546	0.139	0.048	0.000	20.558	−0.058	0.048	1143	2
1100	0.043	20.591	0.138	0.004	0.000	20.618	−0.132	0.004	1145	2
1200	0.027	20.585	0.138	−0.002	0.000	20.568	0.084	−0.002	1143	3
1300	0.039	20.549	0.139	−0.001	0.000	20.592	−0.205	−0.001	1144	2
1400	0.021	20.604	0.138	0.002	0.000	20.646	−0.201	0.002	1147	3
1500	0.013	20.482	0.139	−0.008	0.001	20.310	0.842	−0.008	1133	5
1750	0.005	20.723	0.134	−0.006	0.000	20.788	−0.310	−0.006	1152	16
2000	0.001	20.832	0.140	−0.008	0.006	19.106	8.288	−0.008	1082	57
2400	0.001	20.703	0.141	0.016	0.009	17.934	13.376	0.016	1032	71
2800	0.000	20.804	0.124	−0.546	0.029	12.243	41.153	−0.546	763	371
3200	0.000	21.691	0.099	−1.240	0.011	18.556	14.452	−1.240	1059	231
4000	0.000	29.956	0.160	−0.851	−0.004	31.170	−4.052	−0.851	1534	386

J-value = 0.04301 ± 0.00012
Total gas age = 1141 ± 3 Ma

Power	Fraction	$^{40}Ar/^{39}Ar$	$^{38}Ar/^{39}Ar$	$^{37}Ar/^{39}Ar$	$^{36}Ar/^{39}Ar$	$^{40}Ar^*/^{39}Ar$	%atm	Ca/K	Age (Ma)	1σ error
c3a et105 biotite										
20	0.001	5.768	0.102	−0.095	0.009	3.182	44.831	−0.095	232	123
40	0.000	5.390	0.047	0.873	−0.064	24.228	−349.524	0.873	1289	422
50	0.000	8.230	0.093	−0.360	0.061	−9.819	219.310	−0.360	−990	1530
60	0.000	11.074	0.108	0.519	0.027	3.067	72.300	0.519	224	880
70	0.000	11.343	0.145	0.535	−0.020	17.171	−51.381	0.535	998	395
80	0.000	13.735	0.091	0.146	0.014	9.682	29.507	0.146	628	424
90	0.000	16.344	0.095	−0.080	0.018	11.146	31.808	−0.080	707	413
100	0.000	17.514	0.045	−0.716	−0.008	19.751	−12.768	−0.716	1110	119
110	0.000	18.624	0.059	−0.252	0.003	17.753	4.679	−0.252	1024	112
120	0.001	19.221	0.058	−0.117	0.007	17.199	10.516	−0.117	999	85
130	0.001	20.329	0.065	−0.046	0.007	18.131	10.810	−0.046	1041	48
140	0.002	19.576	0.063	−0.030	0.000	19.662	−0.437	−0.030	1106	26
150	0.003	19.512	0.062	−0.010	−0.001	19.761	−1.279	−0.010	1110	18
160	0.005	19.868	0.061	−0.001	0.000	19.997	−0.649	−0.001	1120	14
170	0.008	19.800	0.063	−0.009	−0.001	20.129	−1.659	−0.009	1126	11
180	0.011	20.104	0.061	0.001	−0.001	20.326	−1.105	0.001	1134	7
190	0.010	20.065	0.065	0.013	0.000	20.059	0.030	0.013	1123	6
200	0.012	20.152	0.066	−0.009	0.000	20.149	0.017	−0.009	1126	6
220	0.017	20.137	0.065	0.006	0.000	20.209	−0.356	0.006	1129	5
240	0.023	20.136	0.065	0.008	0.000	20.120	0.079	0.008	1125	3

Table A.2 (*Continued*)

Power	Fraction	$^{40}Ar/^{39}Ar$	$^{38}Ar/^{39}Ar$	$^{37}Ar/^{39}Ar$	$^{36}Ar/^{39}Ar$	$^{40}Ar^*/^{39}Ar$	%atm	Ca/K	Age (Ma)	1σ error
260	0.027	20.193	0.066	0.004	0.000	20.155	0.186	0.004	1127	3
280	0.029	20.100	0.064	−0.003	0.000	20.158	−0.293	−0.003	1127	3
300	0.032	20.178	0.066	−0.003	0.000	20.217	−0.193	−0.003	1129	2
350	0.045	20.205	0.066	−0.002	0.000	20.196	0.044	−0.002	1128	2
400	0.052	20.258	0.066	−0.002	0.000	20.256	0.013	−0.002	1131	1
480	0.075	20.219	0.065	0.001	0.000	20.207	0.060	0.001	1129	1
560	0.091	20.200	0.064	−0.001	0.000	20.191	0.042	−0.001	1128	1
640	0.120	20.179	0.065	0.002	0.000	20.159	0.101	0.002	1127	1
800	0.268	20.176	0.065	0.002	0.000	20.171	0.027	0.002	1127	1
810	0.055	20.184	0.064	0.000	0.000	20.154	0.150	0.000	1127	2
850	0.038	20.199	0.063	0.000	0.000	20.129	0.346	0.000	1126	2
900	0.031	20.272	0.065	−0.002	0.000	20.248	0.117	−0.002	1131	2
950	0.012	20.225	0.065	−0.002	0.001	19.879	1.712	−0.002	1115	6
1000	0.008	20.350	0.069	−0.014	0.001	20.153	0.967	−0.014	1127	5
1100	0.009	20.410	0.067	−0.006	0.002	19.926	2.371	−0.006	1117	6
1200	0.005	20.813	0.064	−0.033	0.003	20.045	3.687	−0.033	1122	9
1300	0.005	20.450	0.066	0.013	0.003	19.694	3.695	0.013	1107	11
1400	0.002	20.486	0.069	0.011	0.005	19.048	7.017	0.011	1080	23
1500	0.001	20.690	0.075	0.081	−0.008	23.012	−11.220	0.081	1242	78
1750	0.000	23.752	0.046	−0.469	−0.011	26.956	−13.486	−0.469	1389	182
2000	0.000	22.330	0.058	−0.189	−0.003	23.184	−3.822	−0.189	1248	125
2400	0.000	36.859	−0.079	0.737	0.013	33.077	10.261	0.737	1597	943
2800	0.000	46.363	0.026	0.372	0.043	33.690	27.335	0.372	1617	784
3200	0.000	45.511	0.020	1.762	0.223	−20.416	144.860	1.762	−3285	20366
4000	0.000	51.479	0.056	−0.603	0.101	21.723	57.803	−0.603	1191	423

J-value = 0.0430 ± 0.0001
Total gas age = 1126 ± 2 Ma

c2a et103 biotite

50	0.001	14.464	0.068	0.302	0.001	14.204	1.793	0.302	863	39
75	0.001	23.674	0.043	0.180	−0.004	24.854	−4.987	0.180	1315	79
100	0.001	27.886	0.060	0.021	0.003	26.883	3.596	0.021	1390	34
125	0.003	28.324	0.047	0.099	0.000	28.219	0.370	0.099	1437	13
150	0.006	27.580	0.040	0.037	−0.001	27.902	−1.166	0.037	1426	6
175	0.010	27.320	0.041	0.007	0.000	27.381	−0.224	0.007	1407	5
200	0.012	27.412	0.040	−0.001	0.000	27.402	0.038	−0.001	1408	3
225	0.014	27.265	0.040	0.007	0.000	27.210	0.205	0.007	1401	4
250	0.016	27.287	0.040	0.003	0.000	27.216	0.259	0.003	1402	4
275	0.013	27.367	0.040	−0.002	0.000	27.314	0.193	−0.002	1405	4
300	0.003	27.505	0.038	0.001	−0.001	27.676	−0.623	0.001	1418	11
350	0.008	27.347	0.040	0.021	0.000	27.289	0.215	0.021	1404	6
400	0.020	27.360	0.040	0.009	0.000	27.382	−0.080	0.009	1408	2
450	0.033	27.362	0.040	0.001	0.000	27.353	0.034	0.001	1406	1
500	0.040	27.360	0.040	0.006	0.000	27.342	0.063	0.006	1406	2
550	0.047	27.377	0.040	0.005	0.000	27.330	0.171	0.005	1406	2
600	0.051	27.375	0.040	0.008	0.000	27.353	0.079	0.008	1406	2
650	0.049	27.277	0.040	0.008	0.000	27.256	0.079	0.008	1403	1
700	0.050	27.350	0.040	0.019	0.000	27.338	0.043	0.019	1406	1
750	0.043	27.350	0.039	0.028	0.000	27.300	0.186	0.028	1405	2
800	0.040	27.344	0.040	0.038	0.000	27.259	0.311	0.038	1403	2
850	0.040	27.356	0.039	0.038	0.000	27.299	0.212	0.038	1405	1
900	0.049	27.355	0.040	0.024	0.000	27.309	0.167	0.024	1405	2
950	0.039	27.291	0.040	0.031	0.000	27.268	0.086	0.031	1403	2
1000	0.055	27.214	0.039	0.045	0.000	27.178	0.133	0.045	1400	1

Table A.2 (*Continued*)

Power	Fraction	^{40}Ar/^{39}Ar	^{38}Ar/^{39}Ar	^{37}Ar/^{39}Ar	^{36}Ar/^{39}Ar	^{40}Ar*/^{39}Ar	%atm	Ca/K	Age (Ma)	1σ error
1100	0.074	27.302	0.040	0.033	0.000	27.266	0.134	0.033	1403	1
1200	0.185	27.301	0.039	0.026	0.000	27.284	0.061	0.026	1404	3
1300	0.041	27.258	0.040	0.005	0.000	27.263	−0.019	0.005	1403	2
1400	0.029	27.503	0.040	0.000	0.000	27.426	0.281	0.000	1409	2
1600	0.015	27.250	0.039	−0.003	0.000	27.336	−0.315	−0.003	1406	4
1800	0.007	27.391	0.039	−0.005	0.000	27.517	−0.461	−0.005	1412	7
2000	0.004	27.620	0.038	−0.038	−0.001	27.879	−0.936	−0.038	1425	11
2400	0.001	27.850	0.037	−0.075	0.000	27.900	−0.181	−0.075	1426	45
3000	0.000	27.468	0.034	−0.345	−0.008	29.864	−8.721	−0.345	1494	111
4000	0.000	30.546	0.046	−0.767	−0.015	34.918	−14.312	−0.767	1658	253

J-value = 0.0431 ± 0.0001
Total gas age = 1404 ± 2 Ma

a3a et103 hornblende

Power	Fraction	^{40}Ar/^{39}Ar	^{38}Ar/^{39}Ar	^{37}Ar/^{39}Ar	^{36}Ar/^{39}Ar	^{40}Ar*/^{39}Ar	%atm	Ca/K	Age (Ma)	1σ error
100	0.002	6.725	0.088	0.584	0.018	1.420	78.881	0.584	109	65
200	0.000	16.938	0.120	0.275	0.030	7.964	52.981	0.275	540	353
250	0.000	26.718	0.060	0.597	−0.044	39.854	−49.164	0.597	1822	308
300	0.000	23.539	0.118	0.372	−0.038	34.634	−47.134	0.372	1665	322
350	0.000	23.921	0.082	1.375	0.001	23.526	1.653	1.375	1278	177
400	0.000	24.495	0.058	1.040	−0.008	26.834	−9.549	1.040	1402	139
425	0.000	23.545	0.068	1.058	−0.004	24.662	−4.744	1.058	1321	98
450	0.001	23.545	0.089	1.020	−0.012	27.191	−15.482	1.020	1415	137
475	0.000	24.264	0.099	0.917	−0.005	25.784	−6.261	0.917	1364	97
500	0.001	23.465	0.113	1.625	0.006	21.682	7.599	1.625	1205	95
525	0.001	25.145	0.160	1.880	0.007	23.173	7.844	1.880	1264	81
550	0.001	23.827	0.169	1.702	0.005	22.456	5.752	1.702	1236	72
575	0.001	23.658	0.170	2.123	0.003	22.677	4.148	2.123	1244	39
600	0.001	23.523	0.183	2.448	0.004	22.341	5.026	2.448	1231	42
625	0.002	23.335	0.191	2.822	0.003	22.593	3.182	2.822	1241	38
650	0.002	23.018	0.215	3.106	0.003	22.021	4.334	3.106	1218	30
675	0.003	22.995	0.224	3.218	0.002	22.529	2.026	3.218	1239	22
700	0.004	23.142	0.230	3.268	−0.001	23.385	−1.049	3.268	1272	15
725	0.010	23.069	0.239	3.458	0.001	22.725	1.492	3.458	1246	4
750	0.033	23.379	0.244	3.576	0.000	23.371	0.034	3.576	1272	2
775	0.077	23.386	0.244	3.582	0.000	23.377	0.039	3.582	1272	1
800	0.102	23.453	0.244	3.578	0.000	23.477	−0.101	3.578	1276	1
825	0.123	23.332	0.243	3.552	0.000	23.336	−0.015	3.552	1270	1
850	0.140	23.268	0.243	3.551	0.000	23.294	−0.112	3.551	1269	1
875	0.082	23.211	0.243	3.593	0.000	23.250	−0.171	3.593	1267	1
900	0.076	23.182	0.244	3.587	0.000	23.186	−0.015	3.587	1264	1
925	0.059	23.150	0.243	3.567	0.000	23.224	−0.322	3.567	1266	1
950	0.062	23.018	0.244	3.618	0.000	23.055	−0.164	3.618	1259	2
975	0.030	23.122	0.243	3.670	0.000	23.182	−0.260	3.670	1264	3
1000	0.021	23.244	0.248	3.751	0.000	23.199	0.195	3.751	1265	3
1050	0.015	23.271	0.243	3.736	0.000	23.324	−0.226	3.736	1270	5
1100	0.011	23.379	0.250	4.044	−0.001	23.598	−0.935	4.044	1281	8
1150	0.011	23.589	0.248	4.246	0.000	23.588	0.004	4.246	1280	6
1200	0.015	23.384	0.243	3.744	0.000	23.331	0.229	3.744	1270	6
1300	0.006	23.220	0.246	4.012	0.000	23.203	0.070	4.012	1265	9
1400	0.014	22.980	0.247	3.926	0.000	23.121	−0.615	3.926	1262	5
1500	0.005	23.227	0.253	4.410	0.001	22.899	1.412	4.410	1253	13
1750	0.029	22.918	0.247	3.795	0.000	22.932	−0.063	3.795	1254	2
2000	0.023	22.861	0.246	3.929	0.000	22.891	−0.133	3.929	1253	3
2250	0.002	22.216	0.245	3.861	−0.001	22.603	−1.744	3.861	1241	47

Table A.2 (*Continued*)

Power	Fraction	$^{40}Ar/^{39}Ar$	$^{38}Ar/^{39}Ar$	$^{37}Ar/^{39}Ar$	$^{36}Ar/^{39}Ar$	$^{40}Ar^*/^{39}Ar$	%atm	Ca/K	Age (Ma)	1σ error
2500	0.008	22.852	0.245	3.604	0.000	22.774	0.338	3.604	1248	12
3000	0.021	22.514	0.242	3.650	0.000	22.381	0.588	3.650	1233	4
3500	0.004	22.397	0.239	3.596	−0.002	22.948	−2.459	3.596	1255	16
4000	0.001	22.815	0.254	3.833	0.004	21.628	5.205	3.833	1202	93

J-value = 0.0430 ± 0.0001
Total gas age = 1265 ± 3 Ma

c5b et 123 biotite

Power	Fraction	$^{40}Ar/^{39}Ar$	$^{38}Ar/^{39}Ar$	$^{37}Ar/^{39}Ar$	$^{36}Ar/^{39}Ar$	$^{40}Ar^*/^{39}Ar$	%atm	Ca/K	Age (Ma)	1σ error
50	0.003	5.437	0.059	0.022	0.004	4.357	19.862	0.022	309	40
75	0.000	18.972	0.043	−0.153	−0.028	27.314	−43.964	−0.153	1399	180
100	0.001	20.378	0.041	−0.460	0.001	20.027	1.722	−0.460	1119	129
125	0.001	19.530	0.039	0.222	0.007	17.345	11.187	0.222	1004	84
150	0.002	20.432	0.053	−0.002	−0.001	20.746	−1.534	−0.002	1149	47
175	0.003	20.216	0.058	−0.108	−0.003	21.152	−4.628	−0.108	1165	26
200	0.000	21.805	0.001	−1.452	0.001	21.644	0.741	−1.452	1185	469
225	0.000	21.144	0.050	−0.935	−0.003	22.176	−4.882	−0.935	1206	245
250	0.001	20.865	0.045	−0.178	0.011	17.643	15.442	−0.178	1017	87
275	0.001	20.906	0.057	0.013	0.004	19.601	6.245	0.013	1101	43
300	0.002	21.259	0.056	−0.039	0.000	21.380	−0.569	−0.039	1174	28
350	0.023	21.124	0.057	0.011	0.000	21.065	0.280	0.011	1162	3
400	0.036	20.914	0.056	0.005	0.000	20.949	−0.166	0.005	1157	2
450	0.038	20.976	0.056	0.005	0.000	20.997	−0.101	0.005	1159	2
500	0.046	20.943	0.057	0.009	0.000	20.959	−0.076	0.009	1157	2
550	0.058	20.930	0.056	0.003	0.000	20.945	−0.072	0.003	1157	2
600	0.067	20.911	0.056	0.009	0.000	20.889	0.105	0.009	1154	1
650	0.062	20.812	0.056	0.004	0.000	20.792	0.098	0.004	1151	2
700	0.059	20.891	0.057	0.000	0.000	20.835	0.272	0.000	1152	2
750	0.107	20.863	0.056	0.001	0.000	20.860	0.013	0.001	1153	1
800	0.083	20.841	0.057	0.000	0.000	20.829	0.057	0.000	1152	1
850	0.072	20.832	0.055	0.001	0.000	20.845	−0.058	0.001	1153	1
900	0.045	20.814	0.057	0.001	0.000	20.801	0.062	0.001	1151	2
950	0.050	20.884	0.057	−0.002	0.000	20.905	−0.097	−0.002	1155	2
1000	0.034	20.841	0.055	0.004	0.000	20.807	0.165	0.004	1151	3
1100	0.061	20.783	0.056	0.003	0.000	20.714	0.328	0.003	1147	2
1200	0.050	20.799	0.056	0.006	0.000	20.731	0.328	0.006	1148	2
1300	0.018	20.760	0.055	0.005	0.000	20.662	0.476	0.005	1145	4
1400	0.034	20.813	0.056	0.001	0.000	20.773	0.196	0.001	1150	2
1600	0.027	20.865	0.055	0.002	0.000	20.938	−0.350	0.002	1156	5
1800	0.013	20.936	0.057	0.032	0.000	21.069	−0.636	0.032	1162	6
2000	0.002	21.462	0.056	0.003	0.001	21.106	1.660	0.003	1163	45
2400	0.001	21.593	0.046	0.170	−0.005	23.080	−6.891	0.170	1242	96
3000	0.000	26.951	0.029	0.393	0.010	24.084	10.641	0.393	1280	346
4000	0.000	31.813	0.066	0.434	0.048	17.705	44.347	0.434	1020	399

J-value = 0.0429 ± 0.0001
Total gas age = 1151 ± 2 Ma

d3b biotite et 125

Power	Fraction	$^{40}Ar/^{39}Ar$	$^{38}Ar/^{39}Ar$	$^{37}Ar/^{39}Ar$	$^{36}Ar/^{39}Ar$	$^{40}Ar^*/^{39}Ar$	%atm	Ca/K	Age (Ma)	1σ error
50	0.002	25.110	0.029	−0.276	0.029	16.590	33.933	−0.276	567	353
100	0.014	35.993	0.010	−0.055	0.005	34.566	3.964	−0.055	1029	39
200	0.170	37.466	0.012	0.000	0.000	37.393	0.196	0.000	1092	3
275	0.189	37.621	0.013	−0.002	0.000	37.507	0.304	−0.002	1095	3
350	0.124	37.479	0.013	0.011	0.000	37.493	−0.036	0.011	1094	5
425	0.097	37.730	0.013	0.039	0.000	37.599	0.348	0.039	1097	5
500	0.190	37.555	0.012	0.025	0.000	37.507	0.129	0.025	1095	3
575	0.146	37.794	0.012	0.001	0.000	37.869	−0.197	0.001	1102	4

Table A.2 (*Continued*)

Power	Fraction	$^{40}Ar/^{39}Ar$	$^{38}Ar/^{39}Ar$	$^{37}Ar/^{39}Ar$	$^{36}Ar/^{39}Ar$	$^{40}Ar^*/^{39}Ar$	%atm	Ca/K	Age (Ma)	1σ error
650	0.042	37.537	0.013	0.006	−0.001	37.923	−1.029	0.006	1104	14
725	0.012	37.208	0.008	0.056	0.000	37.227	−0.053	0.056	1088	35
1000	0.011	37.545	0.014	−0.001	0.003	36.623	2.455	−0.001	1075	48
3000	0.003	36.957	0.008	0.062	−0.018	42.337	−14.557	0.062	1197	132

J-value = 0.02224 ± 0.00004
Total gas age = 1094.3 ± 2.3 Ma

MI88-b55a 314 hornblende

Power	Fraction	$^{40}Ar/^{39}Ar$	$^{38}Ar/^{39}Ar$	$^{37}Ar/^{39}Ar$	$^{36}Ar/^{39}Ar$	$^{40}Ar^*/^{39}Ar$	%atm	Ca/K	Age (Ma)	1σ error
100	0.003	50.086	0.404	1.381	0.054	34.248	31.622	1.381	1678	12
200	0.012	16.053	0.079	0.688	0.010	13.191	17.832	0.688	838	7
250	0.007	17.683	0.041	0.695	0.006	15.889	10.145	0.695	970	7
300	0.009	22.873	0.034	0.653	0.003	21.930	4.126	0.653	1234	5
350	0.014	18.423	0.032	0.864	0.004	17.288	6.161	0.864	1035	4
400	0.013	20.640	0.029	1.221	0.003	19.895	3.611	1.221	1150	4
425	0.010	21.561	0.031	0.892	0.003	20.720	3.899	0.892	1184	4
450	0.010	21.918	0.033	0.947	0.001	21.568	1.600	0.947	1220	4
475	0.010	23.483	0.038	1.059	0.002	22.959	2.232	1.059	1276	4
500	0.010	20.608	0.041	1.223	0.001	20.194	2.011	1.223	1162	5
525	0.011	19.943	0.046	1.381	0.001	19.577	1.836	1.381	1136	4
550	0.013	19.113	0.051	1.486	0.002	18.571	2.837	1.486	1092	4
575	0.014	19.742	0.061	1.750	0.002	19.245	2.517	1.750	1122	4
600	0.014	19.639	0.071	2.033	0.002	19.169	2.396	2.033	1118	5
625	0.014	20.283	0.084	2.325	0.001	19.868	2.046	2.325	1148	4
650	0.014	20.619	0.097	2.697	0.001	20.199	2.037	2.697	1163	5
675	0.017	21.674	0.144	3.767	0.001	21.355	1.472	3.767	1211	4
700	0.017	21.883	0.151	3.956	0.001	21.688	0.890	3.956	1225	5
725	0.016	21.839	0.152	3.940	0.000	21.697	0.650	3.940	1225	3
750	0.030	23.923	0.232	5.935	0.000	23.806	0.490	5.935	1309	2
775	0.047	24.609	0.263	6.692	0.000	24.550	0.240	6.692	1338	1
800	0.040	24.335	0.258	6.543	0.000	24.231	0.425	6.543	1326	2
825	0.043	24.344	0.265	6.742	0.000	24.328	0.063	6.742	1330	2
850	0.042	24.620	0.265	6.734	0.000	24.533	0.354	6.734	1338	2
875	0.047	25.272	0.269	6.748	0.000	25.198	0.294	6.748	1363	2
900	0.062	25.532	0.280	7.024	0.000	25.466	0.256	7.024	1373	1
925	0.062	25.974	0.277	7.028	0.000	25.890	0.322	7.028	1389	1
950	0.043	25.669	0.263	6.740	0.000	25.559	0.430	6.740	1377	2
975	0.041	25.586	0.258	6.669	0.000	25.510	0.297	6.669	1375	2
1000	0.026	24.578	0.228	5.954	0.001	24.417	0.656	5.954	1333	3
1050	0.034	24.709	0.233	5.924	0.000	24.592	0.474	5.924	1340	2
1100	0.023	23.129	0.198	5.209	0.001	22.967	0.698	5.209	1276	3
1150	0.023	22.826	0.187	4.889	0.001	22.602	0.982	4.889	1262	3
1200	0.019	23.437	0.205	5.483	0.001	23.186	1.070	5.483	1285	3
1300	0.028	25.182	0.209	5.264	0.001	25.007	0.693	5.264	1356	2
1400	0.034	25.299	0.256	6.610	0.001	25.084	0.852	6.610	1359	2
1500	0.021	25.527	0.258	6.968	0.001	25.347	0.705	6.968	1369	2
1750	0.019	25.885	0.257	7.095	0.001	25.562	1.249	7.095	1377	4
2000	0.029	24.697	0.253	7.453	0.001	24.338	1.455	7.453	1330	2
2250	0.035	24.764	0.250	8.007	0.002	24.274	1.978	8.007	1328	2
2500	0.009	20.896	0.186	9.483	0.004	19.800	5.246	9.483	1146	7
3000	0.014	19.372	0.125	7.529	0.004	18.309	5.488	7.529	1080	4
3500	0.000	30.287	0.256	17.604	0.002	29.763	1.728	17.604	1529	113
4000	0.000	21.987	0.152	12.446	−0.049	36.563	−66.292	12.446	1750	408

J-value = 0.0447 ± 0.0003
Total gas age = 1299 ± 5 Ma

Table A.2 (*Continued*)

Power	Fraction	$^{40}Ar/^{39}Ar$	$^{38}Ar/^{39}Ar$	$^{37}Ar/^{39}Ar$	$^{36}Ar/^{39}Ar$	$^{40}Ar^*/^{39}Ar$	%atm	Ca/K	Age (Ma)	1σ error
MI88-b51a 126 biotite										
50	0.003	11.688	0.062	0.189	0.000	11.639	0.414	0.189	757	17
75	0.011	16.591	0.061	0.055	0.000	16.450	0.848	0.055	996	4
100	0.023	20.305	0.065	0.014	0.000	20.232	0.359	0.014	1164	3
125	0.037	21.191	0.067	0.007	0.000	21.180	0.051	0.007	1204	2
150	0.056	21.281	0.066	0.003	0.000	21.274	0.034	0.003	1208	2
175	0.071	21.338	0.066	0.003	0.000	21.335	0.016	0.003	1210	1
200	0.077	21.404	0.066	0.003	0.000	21.405	−0.004	0.003	1213	1
225	0.067	21.488	0.066	0.010	0.000	21.495	−0.031	0.010	1217	1
250	0.052	21.514	0.066	0.020	0.000	21.525	−0.053	0.020	1218	1
275	0.038	21.465	0.066	0.025	0.000	21.452	0.059	0.025	1215	1
300	0.029	21.470	0.066	0.025	0.000	21.569	−0.464	0.025	1220	2
350	0.035	21.366	0.067	0.028	0.000	21.357	0.041	0.028	1211	2
400	0.048	21.328	0.067	0.017	0.000	21.360	−0.151	0.017	1212	1
450	0.070	21.276	0.067	0.012	0.000	21.292	−0.074	0.012	1209	1
500	0.080	21.369	0.066	0.012	0.000	21.367	0.010	0.012	1212	1
550	0.074	21.372	0.066	0.010	0.000	21.369	0.018	0.010	1212	1
600	0.055	21.392	0.067	0.014	0.000	21.414	−0.104	0.014	1214	1
650	0.040	21.469	0.066	0.011	0.000	21.495	−0.121	0.011	1217	1
700	0.037	21.468	0.067	0.015	0.000	21.464	0.020	0.015	1216	1
750	0.027	21.460	0.067	0.021	0.000	21.521	−0.282	0.021	1218	2
800	0.018	21.375	0.066	0.017	0.000	21.407	−0.151	0.017	1213	3
850	0.011	21.393	0.065	0.018	0.000	21.446	−0.245	0.018	1215	4
900	0.011	21.465	0.066	0.030	0.000	21.453	0.058	0.030	1215	5
950	0.007	21.492	0.067	0.045	0.000	21.468	0.110	0.045	1216	6
1000	0.005	21.463	0.067	0.085	0.000	21.399	0.299	0.085	1213	6
1100	0.006	21.538	0.064	0.062	−0.001	21.810	−1.263	0.062	1230	6
1200	0.005	21.657	0.065	0.085	0.000	21.716	−0.273	0.085	1226	7
1300	0.004	21.683	0.066	0.107	−0.001	21.906	−1.026	0.107	1234	7
1400	0.002	21.512	0.062	0.168	0.000	21.497	0.071	0.168	1217	20
1600	0.001	21.548	0.068	0.110	−0.001	21.866	−1.475	0.110	1232	64
1800	0.000	21.214	0.071	0.258	−0.001	21.583	−1.741	0.258	1221	64
2000	0.000	21.916	0.068	−0.042	0.009	19.147	12.637	−0.042	1118	210
2400	0.000	22.411	0.070	−0.010	−0.011	25.793	−15.087	−0.010	1386	110
3000	0.000	21.432	0.071	−0.140	0.037	10.566	50.700	−0.140	699	351
4000	0.000	−1.006	−0.949	2.270	0.193	−58.113	######	2.270	#####	10248

J-value = 0.04482 ± 0.00008

Total gas age = 1208.6 ± 1.6 Ma

Power	Fraction	$^{40}Ar/^{39}Ar$	$^{38}Ar/^{39}Ar$	$^{37}Ar/^{39}Ar$	$^{36}Ar/^{39}Ar$	$^{40}Ar^*/^{39}Ar$	%atm	Ca/K	Age (Ma)	1σ error
MI88-b47a 305b biotite										
50	0.003	8.035	0.216	0.098	0.008	5.735	28.627	0.098	413	21
75	0.003	8.690	0.206	0.015	0.003	7.767	10.619	0.015	540	17
100	0.003	18.823	0.210	−0.010	0.004	17.780	5.542	−0.010	1059	11
125	0.009	19.328	0.200	0.001	0.001	18.982	1.790	0.001	1112	5
150	0.020	20.027	0.201	0.002	0.000	19.894	0.663	0.002	1152	3
175	0.032	20.391	0.203	−0.002	0.000	20.354	0.185	−0.002	1171	1
200	0.023	20.517	0.203	0.000	0.000	20.528	−0.055	0.000	1179	2
225	0.024	20.616	0.202	0.000	0.000	20.630	−0.066	0.000	1183	3
250	0.029	20.649	0.204	0.003	0.000	20.637	0.059	0.003	1183	2
275	0.030	20.650	0.202	−0.002	0.000	20.644	0.026	−0.002	1183	2
300	0.029	20.611	0.203	0.000	0.000	20.656	−0.222	0.000	1184	2
350	0.041	20.716	0.202	0.002	0.000	20.740	−0.113	0.002	1187	1
400	0.047	20.812	0.203	0.001	0.000	20.819	−0.035	0.001	1191	2
450	0.047	20.854	0.203	0.004	0.000	20.852	0.008	0.004	1192	1

Table A.2 (*Continued*)

Power	Fraction	$^{40}Ar/^{39}Ar$	$^{38}Ar/^{39}Ar$	$^{37}Ar/^{39}Ar$	$^{36}Ar/^{39}Ar$	$^{40}Ar^*/^{39}Ar$	%atm	Ca/K	Age (Ma)	1σ error
500	0.047	20.911	0.203	0.003	0.000	20.918	−0.034	0.003	1195	1
550	0.046	20.962	0.204	0.007	0.000	20.964	−0.008	0.007	1197	1
600	0.045	20.972	0.204	0.006	0.000	20.964	0.039	0.006	1197	2
650	0.049	20.982	0.203	0.005	0.000	20.977	0.022	0.005	1197	1
700	0.163	20.975	0.203	0.004	0.000	20.970	0.027	0.004	1197	3
750	0.083	20.704	0.202	0.003	0.000	20.694	0.050	0.003	1186	1
800	0.087	20.672	0.201	0.002	0.000	20.671	0.002	0.002	1185	1
850	0.071	20.615	0.202	0.002	0.000	20.609	0.028	0.002	1182	1
900	0.035	20.621	0.200	0.001	0.000	20.632	−0.055	0.001	1183	1
950	0.016	20.657	0.200	−0.016	0.000	20.637	0.096	−0.016	1183	3
1000	0.006	20.519	0.200	−0.051	0.000	20.604	−0.411	−0.051	1182	6
1100	0.004	20.695	0.198	−0.078	−0.001	20.894	−0.961	−0.078	1194	11
1200	0.004	20.834	0.196	−0.071	0.000	20.697	0.657	−0.071	1186	10
1300	0.001	20.554	0.199	−0.245	0.002	20.005	2.674	−0.245	1156	24
1400	0.001	20.908	0.203	−0.137	0.002	20.452	2.181	−0.137	1175	22
1600	0.000	20.360	0.200	0.117	−0.006	22.194	−9.010	0.117	1247	125
1800	0.000	20.820	0.211	0.042	0.011	17.638	15.280	0.042	1052	117
2000	0.001	21.325	0.210	0.170	0.004	20.276	4.918	0.170	1168	70
2400	0.001	21.186	0.201	0.100	0.002	20.487	3.299	0.100	1177	63
3000	0.000	21.472	0.193	0.356	0.008	19.243	10.378	0.356	1124	151
4000	0.000	23.304	0.194	0.176	0.044	10.268	55.937	0.176	684	577

J-value = 0.04491 ± 0.00009
Total gas age = 1183.4 ± 1.8 Ma

MI88-b46a 122 biotite

Power	Fraction	$^{40}Ar/^{39}Ar$	$^{38}Ar/^{39}Ar$	$^{37}Ar/^{39}Ar$	$^{36}Ar/^{39}Ar$	$^{40}Ar^*/^{39}Ar$	%atm	Ca/K	Age (Ma)	1σ error
50	0.004	4.827	0.114	0.540	0.003	3.841	20.427	0.540	287	11
75	0.009	4.837	0.094	0.141	0.001	4.489	7.187	0.141	331	7
100	0.007	14.770	0.133	0.055	0.002	14.192	3.918	0.055	890	7
125	0.018	16.720	0.143	0.030	0.001	16.536	1.100	0.030	1002	2
150	0.029	18.395	0.152	0.012	0.000	18.321	0.400	0.012	1083	2
175	0.034	18.858	0.155	0.010	0.000	18.833	0.130	0.010	1106	1
200	0.043	18.961	0.156	0.010	0.000	19.006	−0.235	0.010	1114	1
225	0.051	19.046	0.157	0.008	0.000	19.072	−0.138	0.008	1116	1
250	0.055	19.068	0.157	0.009	0.000	19.071	−0.015	0.009	1116	1
275	0.057	19.124	0.157	0.012	0.000	19.149	−0.132	0.012	1120	1
300	0.053	19.128	0.157	0.013	0.000	19.152	−0.124	0.013	1120	1
350	0.069	19.236	0.159	0.026	0.000	19.229	0.037	0.026	1123	1
400	0.071	19.395	0.158	0.030	0.000	19.427	−0.165	0.030	1132	1
450	0.072	19.439	0.158	0.039	0.000	19.471	−0.165	0.039	1134	1
500	0.089	19.179	0.158	0.038	0.000	19.186	−0.034	0.038	1121	1
550	0.095	19.007	0.156	0.051	0.000	19.014	−0.038	0.051	1114	1
600	0.059	18.957	0.156	0.037	0.000	18.963	−0.034	0.037	1112	1
650	0.036	18.954	0.156	0.012	0.000	18.977	−0.120	0.012	1112	2
700	0.040	18.910	0.155	0.038	0.000	18.962	−0.274	0.038	1112	1
750	0.026	18.948	0.155	0.010	0.000	19.017	−0.363	0.010	1114	2
800	0.016	18.930	0.156	0.014	0.000	19.010	−0.421	0.014	1114	3
850	0.011	18.937	0.154	0.001	0.000	19.018	−0.426	0.001	1114	5
900	0.010	18.966	0.154	0.015	0.000	19.077	−0.585	0.015	1117	5
950	0.008	18.983	0.155	0.064	0.000	18.981	0.010	0.064	1112	7
1000	0.007	18.975	0.156	0.009	0.000	18.874	0.531	0.009	1108	7
1100	0.012	18.987	0.154	0.053	0.000	19.019	−0.169	0.053	1114	4
1200	0.006	18.937	0.151	0.014	0.000	18.910	0.145	0.014	1109	11
1300	0.004	18.912	0.153	0.026	0.000	18.854	0.308	0.026	1107	12
1400	0.003	18.873	0.155	0.038	0.001	18.519	1.877	0.038	1092	16

Table A.2 (*Continued*)

Power	Fraction	$^{40}Ar/^{39}Ar$	$^{38}Ar/^{39}Ar$	$^{37}Ar/^{39}Ar$	$^{36}Ar/^{39}Ar$	$^{40}Ar^*/^{39}Ar$	%atm	Ca/K	Age (Ma)	1σ error
1600	0.003	18.745	0.151	0.020	−0.001	18.991	−1.314	0.020	1113	9
1800	0.001	17.972	0.130	0.025	−0.004	19.181	−6.725	0.025	1121	47
2000	0.000	15.787	0.084	0.404	−0.036	26.512	−67.943	0.404	1415	327
2400	0.000	18.686	0.043	0.652	−0.043	31.375	−67.903	0.652	1587	736
3000	0.000	23.269	1.269	16.929	0.430	−103.722	545.759	16.929	#####	16472
4000	0.000	0.126	0.082	−0.459	0.579	−171.038	######	−0.459	####	2035

J-value = 0.04492 ± 0.00009
Total gas age = 1105.2 ± 1.7 Ma

MI88-b45a 308a biotite

Power	Fraction	$^{40}Ar/^{39}Ar$	$^{38}Ar/^{39}Ar$	$^{37}Ar/^{39}Ar$	$^{36}Ar/^{39}Ar$	$^{40}Ar^*/^{39}Ar$	%atm	Ca/K	Age (Ma)	1σ error
50	0.005	8.318	0.035	0.052	0.005	6.895	17.109	0.052	487	23
75	0.002	16.713	0.005	0.033	0.000	16.814	−0.601	0.033	1015	23
100	0.003	18.289	0.007	0.077	0.000	18.190	0.543	0.077	1078	20
125	0.006	19.226	0.004	0.009	0.000	19.329	−0.538	0.009	1128	13
150	0.012	18.892	0.008	−0.018	0.000	18.762	0.685	−0.018	1103	10
175	0.020	18.918	0.009	0.010	0.001	18.688	1.213	0.010	1100	4
200	0.027	18.792	0.008	0.030	0.001	18.561	1.228	0.030	1094	5
225	0.028	18.816	0.010	0.003	0.000	18.733	0.439	0.003	1102	5
250	0.029	18.767	0.009	0.009	0.000	18.651	0.617	0.009	1098	5
275	0.033	18.798	0.010	0.010	0.000	18.824	−0.137	0.010	1106	4
300	0.034	18.815	0.011	0.017	0.000	18.747	0.359	0.017	1103	5
350	0.049	18.943	0.012	0.017	0.000	18.934	0.047	0.017	1111	3
400	0.055	19.091	0.013	0.012	0.000	19.049	0.223	0.012	1116	3
450	0.056	18.970	0.014	0.009	0.000	18.991	−0.110	0.009	1113	3
500	0.065	19.059	0.015	0.010	0.000	19.041	0.095	0.010	1116	2
550	0.065	18.986	0.014	0.005	0.000	18.970	0.085	0.005	1112	2
600	0.074	18.914	0.014	0.006	0.000	18.903	0.059	0.006	1109	2
650	0.057	18.957	0.015	0.003	0.000	18.937	0.104	0.003	1111	2
700	0.090	19.159	0.015	0.004	0.000	19.153	0.035	0.004	1120	1
750	0.067	19.219	0.015	0.005	0.000	19.168	0.263	0.005	1121	2
800	0.023	19.047	0.013	0.007	0.000	18.964	0.432	0.007	1112	5
850	0.123	19.325	0.017	−0.001	0.000	19.333	−0.042	−0.001	1128	1
900	0.021	19.327	0.006	0.003	0.000	19.347	−0.099	0.003	1129	6
950	0.007	19.028	0.008	−0.031	0.000	19.077	−0.257	−0.031	1117	21
1000	0.016	19.511	0.010	0.001	0.000	19.457	0.279	0.001	1134	9
1100	0.000	19.511	−0.469	4.684	0.019	13.798	29.281	4.684	871	4336
1200	0.000	23.121	−0.186	4.624	0.241	−47.972	307.485	4.624	#####	4493
1300	0.000	18.085	−0.017	−3.497	0.001	17.743	1.896	−3.497	1058	2678
1400	0.000	22.556	−0.032	2.322	0.080	−1.059	104.695	2.322	−88	5125
1600	0.006	19.771	0.012	0.015	−0.001	20.205	−2.192	0.015	1166	15
1800	0.012	19.952	0.009	0.024	0.000	19.992	−0.200	0.024	1157	8
2800	0.012	19.503	0.012	0.010	0.000	19.541	−0.194	0.010	1137	9
4000	0.002	21.271	−0.001	−0.014	−0.006	23.137	−8.772	−0.014	1286	60

J-value = 0.04495 ± 0.00009
Total gas age = 1113.3 ± 1.9 Ma

MI88-b44a 314 biotite

Power	Fraction	$^{40}Ar/^{39}Ar$	$^{38}Ar/^{39}Ar$	$^{37}Ar/^{39}Ar$	$^{36}Ar/^{39}Ar$	$^{40}Ar^*/^{39}Ar$	%atm	Ca/K	Age (Ma)	1σ error
50	0.001	13.185	0.059	0.197	0.007	10.999	16.581	0.197	725	20
75	0.001	16.230	0.041	0.150	0.002	15.575	4.036	0.150	958	15
100	0.004	12.738	0.033	0.138	0.001	12.462	2.170	0.138	803	6
125	0.005	20.194	0.036	0.077	0.001	20.016	0.884	0.077	1158	5
150	0.007	26.556	0.039	0.014	0.001	26.260	1.113	0.014	1407	3
175	0.012	27.115	0.040	0.010	0.001	26.725	1.437	0.010	1424	2
200	0.019	27.072	0.040	0.006	0.000	26.956	0.428	0.006	1432	2

Table A.2 (*Continued*)

Power	Fraction	$^{40}Ar/^{39}Ar$	$^{38}Ar/^{39}Ar$	$^{37}Ar/^{39}Ar$	$^{36}Ar/^{39}Ar$	$^{40}Ar^*/^{39}Ar$	%atm	Ca/K	Age (Ma)	1σ error
225	0.028	27.393	0.040	0.005	0.000	27.286	0.391	0.005	1445	1
250	0.034	27.603	0.039	0.004	0.000	27.570	0.121	0.004	1455	1
275	0.036	27.630	0.039	0.005	0.000	27.567	0.227	0.005	1455	1
300	0.036	27.819	0.039	0.008	0.000	27.784	0.128	0.008	1463	1
350	0.053	27.795	0.039	0.006	0.000	27.809	−0.049	0.006	1463	1
400	0.053	27.754	0.039	0.008	0.000	27.764	−0.035	0.008	1462	1
450	0.049	27.834	0.039	0.010	0.000	27.841	−0.023	0.010	1465	1
500	0.045	27.907	0.040	0.012	0.000	27.934	−0.094	0.012	1468	1
550	0.045	27.956	0.040	0.015	0.000	27.983	−0.097	0.015	1470	1
600	0.046	27.847	0.040	0.016	0.000	27.854	−0.025	0.016	1465	1
650	0.045	27.817	0.040	0.017	0.000	27.816	0.004	0.017	1464	1
700	0.042	27.768	0.040	0.019	0.000	27.773	−0.020	0.019	1462	1
750	0.043	27.722	0.040	0.021	0.000	27.721	0.004	0.021	1460	1
800	0.051	27.688	0.039	0.016	0.000	27.674	0.051	0.016	1459	1
850	0.052	27.683	0.039	0.020	0.000	27.674	0.033	0.020	1459	1
900	0.040	27.689	0.039	0.031	0.000	27.697	−0.030	0.031	1459	1
950	0.050	27.726	0.039	0.011	0.000	27.713	0.047	0.011	1460	1
1000	0.030	27.729	0.038	0.011	0.000	27.714	0.055	0.011	1460	1
1100	0.032	27.751	0.039	0.019	0.000	27.742	0.030	0.019	1461	1
1200	0.028	27.641	0.039	0.021	0.000	27.620	0.074	0.021	1457	1
1300	0.019	27.674	0.039	0.043	0.000	27.668	0.021	0.043	1458	1
1400	0.019	27.699	0.039	0.023	0.000	27.692	0.028	0.023	1459	1
1600	0.022	27.606	0.039	0.053	0.000	27.584	0.078	0.053	1455	2
1800	0.047	27.639	0.040	0.131	0.000	27.638	0.004	0.131	1457	1
2000	0.003	27.481	0.040	0.076	−0.001	27.650	−0.616	0.076	1458	7
2400	0.001	27.889	0.043	0.011	−0.002	28.419	−1.900	0.011	1485	27
3000	0.001	27.560	0.038	0.107	0.000	27.676	−0.422	0.107	1459	17
4000	0.000	27.905	0.077	0.956	0.022	21.335	23.543	0.956	1214	527

J-value = 0.04497 ± 0.00009
Total gas age = 1454.5 ± 2.1 Ma

References

Almeida, F.F.M., Hasui, Y., 1984. O embasamento da plataforma Sul Americana, in: Almeida, F.F.M., Hasui, Y. (Eds.), O Precambriano do Brasil, Editora Edgard Blücher, São Paulo.

Amaral, G., 1974. Geologia Pré-Cambriana da região Amazônica, Unpublished Ph.D. Thesis, Universidade de São Paulo, 144 p. (in Portuguese).

Barros, A.M., Silva, R.H., Cardoso, O.R.F., Freire, F.A., Souza, J.J., Rivetti, M., Luz, D.S., Barros Palmeira, R.C., Tassinari, C.C.G., 1982, Projeto RADAMBRASIL; Folha SD.21 Cuiabá, Geologia, geomorfologia, pedologia, vegetação, e uso potencial da terra, Translated title: Geology, geomorphology, pedology, vegetation, and potential uses of land, Ministério das Minas e Energia, Rio de Janeiro, 544 p.

Bettencourt, J.S., Onstott, T.C., de Jesus, T., Teixeira, W., 1996. Tectonic interpretation of $^{40}Ar/^{39}Ar$ ages of country rocks from the central sector of the Río Negro–Juruena Province, southwest Amazonian craton. Int. Geol. Rev. 38, 42–56.

Bettencourt, J.S., Tosdal, R.M., Leite, W.B., Payolla, B.L., 1999. Mesoproterozoic rapakivi granites of the Rondônia tin province, southwestern border of the Amazonian Craton, Brazil: reconnaissance U–Pb geochronology and regional implications. Precam. Res. 95, 41–67.

Busch, J.P., Mezger, K., van der Pluijm, B.A., 1997. Suturing and extensional reactivation in the Grenville orogen, Canada. Geology 25, 507–510.

Carrigan, C.W., Miller, C.F., Fullagar, P.D., Bream, B.R., Hatcher, R.D., Coath, C.D., 2003. Ion microprobe ages and geochemistry of southern Appalachian basement, with implications for Proterozoic and Paleozoic reconstructions. Precam. Res. 120, 1–36.

Cordani, U.G., Sato, K., 1999. Crustal evolution of the South American Platform, based on Nd isotopic systematics on granitoid rocks. Episodes 22, 167–173.

Davidson, A., 1998. An overview of Grenville Province geology, Canadian Shield. In Lucas, S.B., St-Onge, M.R., (Eds.), Geology of the Precambrian Superior Province and Precambrian fossils in North America. vol. 7. Geol. Surv. Can., pp. 205–270.

Davidson, J., Charlier, B., Hora, J.M., Perlroth, R., 2005. Mineral isochrons and isotopic fingerprinting: pitfalls and promises. Geology 33, 29–32.

Fernandes, C.J., 1999. Geologia do depósito Pau-a-Piques e guias prospectivos para ouro no Grupo Aguapeí, sudoeste do estado de Mato Grosso, unpublished M.Sc., Universidade Federal do Rio Grande do Sul, Porto Allegre, 134 p. (in Portuguese).

Geraldes, M.C., Figueiredo, B.R., Tassinari, C.C.G., Ebert, H.D., 1997. Middle Proterozoic vein hosted gold deposits in the Pontes e Lacerda region, southwestern Amazonian craton, Brazil. Int. Geol. Rev. 39, 438–448.

Geraldes, M.C., Van Schmus, W.R., Condie, K.C., Bell, S., Teixeira, W., Babinski, M., Bartley, J.K., Kah, L.C., 2001. Proterozoic geologic evolution of the SW part of the Amazonian Craton in Mato Grosso State, Brazil. Precam. Res. 111, 91–128.

Heaman, L., Parrish, R.R., 1991. U-Pb geochronology of accessory minerals. Short Course Handbook, vol. 19. Mineralogical Association of Canada, pp. 59–102.

Hoffman, P.F., 1991. Did the breakout of Laurentia turn Gondwana inside out? Science 252, 1409–1412.

Ketchum, J.W.F., Heaman, L.M., Krogh, T.E., Culshaw, N.G., Jamieson, R.A., 1998. Timing and therman influence of late orogenic extension in the lower crust: a U–Pb geochronological study from the southwest Grenville orogen. Can. Precam. Res. 89, 25–45.

Leal, J.W.L., Silva, G.H., Santos, D.B., Teixeira, W., de Lima, M.I.C., Fernandes, C.A.C., Pinto, A., 1978. Folha SC. 20, Porto Velho, [Monograph] Projeto RADAMBRASIL, Departamento Nacional de Producao Mineral, Rio de Janeiro, 16, pp. 17–184 (in Portuguese).

Litherland, M., Bloomfield, K., 1981. The Proterozoic history of eastern Bolivia. Precam. Res. 15, 157–161.

Litherland, M., Annells, R.N., Appleton, J.D., Berrange, J.P., Bloomfield, K., Burton, C.C.J., Darbyshire, D.P.F., Fletcher, C.J.N., Hawkins, M.P., Klinck, B.A., Llanos, A., Mitchell, W.I., O'Connor, E.A., Pitfield, P.E.J., Power, G., Webb, B.C., 1986. The geology and mineral resources of the Bolivian Precambrian shield. British Geological Survey Overseas Memoir, vol. 9, 153 pp.

Litherland, M., Annells, R.N., Darbyshire, D.P.F., Fletcher, C.J.N., Hawkins, M.P., Klinck, B.A., Mitchell, W.I., O'Connor, E.A., Pitfield, P.E.J., Power, G., Webb, B.C., 1989. The Proterozoic of eastern Bolivia and its relationship to the Andean mobile belt. Precam. Res. 43, 157–174.

Loewy, S., Connelly, J.N., Dalziel, L.W.D., Gower, C.F., 2003. Amazonia in Rodinia: constraints from whole rock Pb and U/Pb geochronology. Tectonophysics 375, 169–197.

Mezger, K., van der Pluijm, B.A., Essene, E.J., Halliday, A.N., 1992. The Carthage-Colton mylonite zone (Adirondack Mountains, New York): the site of a cryptic suture in the Grenville Orogen? J. Geol. 100, 630–638.

Mezger, K., Essene, E.J., van der Pluijm, B.A., Halliday, A.N., 1993. U–Pb geochronology of the Grenville Orogen of Ontario and New York: constraints on ancient crustal tectonics. Contrib. Miner. Petrol. 114, 13–26.

Parrish, R.R., 1991. U–Pb dating of monazite and its application to geological problems. Can. J. Earth Sci. 27, 1435–1450.

Payolla, B.L., Bettencourt, J.S., Kozuch, M., Leite Jr., W.B., Fetter, A.H., Van Schmus, W.R., 2002. Geological evolution of the basement rocks in the east-central part of the Rondônia Tin Province, SW Amazon craton, Brazil: U–Pb and Sm–Nd isotopic constraints. Precam. Res. 119, 141–169.

Pinho, M.A.S.B., Chemale, F., Van Schmus, W.R., Pinho, F.E.C., 2003. U–Pb and Sm–Nd evidence for 1.76–1.77 Ga magmatism in the Moriru region, Mato Grosso, Brazil: implications for province boundaries in the SW Amazon Craton. Precam. Res. 126, 1–25.

Priem, H.N.A., Boelrijk, N.A.I.M., Hebeda, E.H., Verdurmen, E.A.Th., Verschure, R.H., Bon, E.H., 1971. Granitic complexes and associated tin mineralizations of "Grenville" age in Rondônia, western Brazil. Geol. Soc. Am. Bull. 82, 1095–1102.

Priem, H.N.A., Bon, E.H., Verdurmen, E.A.Th., Bettencourt, J.S., 1989. Rb–Sr geochronology of Precambrian crustal evolution in Rondônia (western margin of the Amazonian craton), Brazil. J. S. Am. Earth Sci. 2, 163–170.

Provost, A., 1990. An improved diagram for isochron data. Chem. Geol. 80, 85–99.

Rivers, T., 1997. Lithotectonic elements of the Grenville Province: review and tectonic implications. Precam. Res. 86, 117–154.

Rizzotto, G.J., 1999. Petrologia e geotectônia do Grupo Nova Brasilândia, Rondônia. Unpublished M.Sc., Universidade Federal do Rio Grande do Sul, Porto Allegre, 131 p. (in Portuguese).

Rizzotto, G.J., 2001, Reavaliação do ciclo orogênico Sunsás/Aguapeí no sudoeste do craton Amazônico, Workshop of the SW Amazonian Craton: State of the Art Universidade de São Paulo, São Paulo, Brazil, August 10–12.

Rizzotto, G.J., Quadros, M.L.E.S., Scandolara, J.E., Silva, C.R., Bahia, R.B.C., 1995. Posicionamento tectono-estratigráfico da sequência metavulcano-sedimentar Roosevelt na região limítrofe dos estados de Rondônia e Mato Grosso, 5th Simpósio Nacional de Estudos Tectônicos, Gramado, pp. 310–311 (in Portuguese).

Rizzotto, G.J., Chemale, F., de Lima, E.F., Van Schmus, R., Fetter, A., 1999. Sm/Nd and U/Pb isotopic data for the Nova Brasilândia metaplutonic, metavolcanosedimentary sequence, Rondônia. Annual 70th Meeting Brazilian Geology Society, Salvador, 1998.

Rougvie, J.R., Carlson, W.D., Copeland, P., Connelly, J.N., 1999. Late thermal evolution of Proterozoic rocks in the northeastern Llano Uplift, central Texas. Precam. Res. 94, 49–72.

Sadowski, G.R., Bettencourt, J.S., 1996. Mesoproterozoic tectonic correlations between eastern Laurentia and the western border of the Amazon craton. Precam. Res. 76, 213–227.

Saes, G.S., 1999. Tectonic and paleogeographic evolution of the Aguapeí aulacogen (1.2–1.0 Ga) and the basement terranes in the southern Amazon craton. Ph.D. Thesis, Universidade de São Paulo, 135 p. (in Portuguese).

Scandolâra, J.E., Rizzotto, G.J., de Amorim, J.L., Bahia, R.B.C., Quadros, M.L., Silva, C.R., 1998. Geological map of Rondônia 1:1,000,000, Companhia de Pesquisa de Recursos Minerais.

Stacey, J.S., Kramers, J.D., 1975. Approximation of terrestrial lead isotopic evolution by a two-stage model. Earth Planet. Sci. Lett. 26, 207–221.

Streepey, M.M., Johnson, E.L., Mezger, K., van der Pluijm, B.A., 2001. Early history of the Carthage-Colton shear zone, Grenville

Province, Northwest Adirondacks, New York (USA). J. Geol. 109, 479–492.

Tassinari, C.C.G., 1981. Evolução geotectônica da Província Rio-Negro-Juruena na região Amazônica. Unpublished M.Sc., Universidade de São Paulo, 99 p. (in Portuguese).

Tassinari, C.C.G., Macambira, M.J.B., 1999. Geochronological provinces of the Amazonian Craton. Episodes 22, 174–182.

Tassinari, C.C.G., Cordani, U.G., Nutman, A.P., Van Schmus, W.R., Bettencourt, J.S., Taylor, P.N., 1996. Geochronological systematics on basement rocks from the Rio Negro-Juruena Province (Amazonian Craton) and tectonic implications. Int. Geol. Rev. 38, 161–175.

Tassinari, C.C.G., Bettencourt, J.S., Geraldes, M.C., Macambira, M.J.B., Lafon, J.M., 2000. The Amazonian craton, in Tectonic evolution of South America. In: Cordani, U.G., Milani, E.J., Thomaz Filho, A., Campos, D.A. (Eds.), Rio de Janeiro, pp. 41–95.

Teixeira, W., Tassinari, C.C.G., Cordani, U.G., Kashawita, K., 1989. A review of the geochronology of the Amazonian craton: tectonic implications. Precam. Res. 42, 213–227.

Tohver, E., van der Pluijm, B.A., Van der Voo, R., Rizzotto, G., Scandolara, J.E., 2002. Paleogeography of the Amazon craton at 1.2 Ga: early Grenvillian collision with the Llano segment of Laurentia. Earth Planet. Sci. Lett. 199, 185–200.

Tohver, E., Bettencourt, J.S., Tosdal, R., Mezger, K., Leite, W.B., Payolla, B.L., 2004. Terrane transfer during the Grenville orogeny: tracing the Amazonian ancestry of southern Appalahian basement through Pb and Nd isotopes. Earth Planet. Sci. Lett. 228, 161–176, 10.1016/j.epsl.2004.09.029.

Tohver, E., van der Pluijm, B.A., Mezger, K., Scandolara, J.E., Essene, E.J., Significance of the Nova Brasilândia Metasedimentary Belt in western Brazil: Redefining the Mesoproterozoic boundary of the Amazon craton. Tectonics 23, TC6004.

Tohver, E., van der Pluijm, B.A., Scandolara, J.E., Essene, E.J. Grenville-aged deformation of Amazonia (Rondônia, Brazil): evidence for oblique collision with southern Laurentia. J. Geol., in press.

Tosdal, R.M., Bettencourt, J.S., 1994. U–Pb zircon ages and Pb isotopic compositions of middle Proterozoic Rondônian massifs, southwestern margin of the Amazon craton, Brazil, Actas, Seventh Congresso Geológico Chileno, pp. 1538–1541.

van der Pluijm, B.A., Mezger, K., Cosca, M.A., Essene, E.J., 1994. Determining the significance of high grade shear zones. Geology 22, 743–746.

Weil, A.B., Van der Voo, R., Connall, Mac-Niocaill, Meert, J.G., 1998. The Proterozoic supercontinent Rodinia; paleomagnetically derived reconstruction for 1100 to 800 Ma. Earth Planet. Sci. Lett. 154, 13–24.